[12.7.2019–7:09pm] [1–19] Paper: OP-BRAI190237
SUBJECT CATEGORY: ORIGINAL ARTICLE MANUSCRIPT CATEGORY: ORIGINAL ARTICLE

BRAIN
A JOURNAL OF NEUROLOGY

Increased translation as a novel pathogenic mechanism in Huntington's disease

Jordi Creus-Muncunill,[1,2,3] Raquel Badillos-Rodríguez,[1,2,3] Marta Garcia-Forn,[1,2,3] Mercè Masana,[1,2,3] Gerardo Garcia-Díaz Barriga,[1,2,3] Anna Guisado-Corcoll,[1,2,3] Jordi Alberch,[1,2,3] Cristina Malagelada,[1] José M. Delgado-García,[4] Agnès Gruart[4] and Esther Pérez-Navarro[1,2,3]

AQ1

See Brouillet (doi:10.1093/brain/awzxxx) for a scientific commentary on this article.

Huntington's disease is a neurodegenerative disorder caused by a CAG repeat expansion in the exon-1 of the huntingtin gene. Striatal projection neurons are mainly affected, leading to motor symptoms, but molecular mechanisms involved in their vulnerability are not fully characterized. Here, we show that eIF4E binding protein (4E-BP), a protein that inhibits translation, is inactivated in Huntington's disease striatum by increased phosphorylation. Accordingly, we detected aberrant *de novo* protein synthesis. Proteomic characterization indicates that translation specifically affects sets of proteins as we observed upregulation of ribosomal and oxidative phosphorylation proteins and downregulation of proteins related to neuronal structure and function. Interestingly, treatment with the translation inhibitor 4EGI-1 prevented R6/1 mice motor deficits, although corticostriatal long-term depression was not markedly changed in behaving animals. At the molecular level, injection of 4EGI-1 normalized protein synthesis and ribosomal content in R6/1 mouse striatum. In conclusion, our results indicate that dysregulation of protein synthesis is involved in mutant huntingtin-induced striatal neurons dysfunction.

1 Departament de Biomedicina, Facultat de Medicina i Ciències de la Salut, Institut de Neurociències, Universitat de Barcelona, 08036 Barcelona, Catalonia
2 Institut d'Investigacions Biomèdiques August Pi i Sunyer (IDIBAPS), Barcelona, Catalonia
AQ8 3 Centro de Investigación Biomédica en Red sobre Enfermedades Neurodegenerativas (CIBERNED), Spain
AQ2 4 Division of Neurosciences, Pablo de Olavide University, Seville, Spain

Correspondence to: Esther Pérez-Navarro
Departament de Biomedicina, Facultat de Medicina i Ciències de la Salut, Institut de Neurociències, Universitat de Barcelona, 08036 Barcelona, Catalonia
E-mail: estherperez@ub.edu

Keywords: 4E-BP1; striatum; ribosomal proteins; long-term depression; 4EGI-1

Abbreviations: 4E-BP1 = eIF4E binding protein; eIF4F = eukaryotic translation initiation factor 4F; Htt = huntingtin; LFS = low frequency stimulation; LTD = long-term depression; mTOR = mechanistic target of rapamycin

Introduction

Huntington's disease is a progressive neurodegenerative disorder characterized by motor and cognitive impairment (Martin and Gusella, 1986). It is caused by a CAG trinucleotide repeat expansion within the exon 1 of the Huntingtin (Htt) gene, which leads to lengthening of the polyglutamine chain in the N-terminus of the translated protein (HDCRG, 1993). The result is an aberrant and misfolded mutant protein (mHtt) associated with protein

Received December 28, 2018. Revised May 29, 2019. Accepted June 2, 2019.
© The Author(s) (2019). Published by Oxford University Press on behalf of the Guarantors of Brain. All rights reserved.
For Permissions, please email: journals.permissions@oup.com

[12.7.2019–7:09pm] [1–19] Paper: OP-BRAI190237
SUBJECT CATEGORY: ORIGINAL ARTICLE MANUSCRIPT CATEGORY: ORIGINAL ARTICLE

aggregation and toxicity. Although mHtt expression is ubiquitous in the brain, the most vulnerable region is the striatum (Han *et al.*, 2010). The molecular basis that accounts for this specific neurodegeneration is still not clear, but different mechanisms have been proposed to contribute to the neurodegenerative process (Labbadia and Morimoto, 2013). Expression of mHtt disrupts the normal signalling of many intracellular pathways (Bowles and Jones, 2014), and it also induces the activation of compensatory mechanisms to prevent or delay cell dysfunction and apoptosis (Kreiner, 2015). Many intracellular pathways altered in Huntington's disease participate in the regulation of protein translation (Wang and Proud 2006; Osterweil *et al.*, 2010; Wiseman *et al.*, 2013), namely the mechanistic target of rapamycin (mTOR) (Pryor *et al.*, 2014; Lee *et al.*, 2015), ERK1/2 (Saavedra *et al.*, 2011) and PKA pathways (Tyebji *et al.*, 2015). Interestingly, increased protein synthesis has been associated with neuronal toxicity or dysfunction occurring in some neurological and neurodegenerative disorders (Sharma *et al.*, 2010; Santini *et al.*, 2013; Baleriola *et al.*, 2014; Martin *et al.*, 2014*a*; Topol *et al.*, 2015).

The initiation of protein synthesis is controlled by the eukaryotic translation initiation factor 4F (eIF4F) complex, composed of the cap-binding protein eIF4E, the RNA helicase eIF4A and the scaffolding protein eIF4G that recruits the mRNA to the ribosome. The main regulator of this complex is the eIF4E binding protein (4E-BP), which binds to and inactivates eIF4E. The phosphorylation of 4E-BP disrupts its interaction with eIF4E, which can then interact with eIF4G and eIF4A to form the eIF4F complex, responsible for cap-dependent translation initiation (Pause *et al.*, 1994). Phosphorylation of 4E-BP occurs initially at Thr37/Thr46 by the mTOR complex 1 (mTORC1), which is sufficient to block its association with eIF4E. Subsequent phosphorylation occurs at Thr70 followed by Ser65 (Gingras *et al.*, 1999). In addition to mTORC1, GSK3β can also fully phosphorylate 4E-BP (Ito *et al.*, 2016). Thus, altered 4E-BP phosphorylation may cause an alteration in the translational control and, consequently, an exaggerated and aberrant protein synthesis.

In Huntington's disease striatum, the activity of mTORC1 and GSK3β are altered (Ravikumar *et al.*, 2004; Valencia *et al.*, 2010; Lim *et al.*, 2014; Pryor *et al.*, 2014; Fernández-Nogales *et al.*, 2015; Lee *et al.*, 2015, 2016), which suggests a possible impact on 4E-BP phosphorylation and consequently on translation. Therefore, here we investigated whether 4E-BP phosphorylation is altered in the striatum of Huntington's disease and its consequences for protein synthesis and neuronal function.

Materials and methods

Huntington's disease mouse models

Male R6/1 and R6/2 heterozygous transgenic mice (B6CBA background) expressing the exon-1 of mHtt with 145 and 90 CAG repeats, respectively, and homozygous mutant $Hdh^{Q111/Q111}$, with targeted insertion of 109 CAG repeats that extends the glutamine segment in murine huntingtin to 111 residues and wild-type $Hdh^{Q7/Q7}$knock-in mice were used. Genotyping and CAG repeat length determination were performed as previously described (Giralt *et al.*, 2011). All mice were housed together in numerical birth order in groups of mixed genotypes, and data were recorded for analysis by microchip mouse number. Experiments were conducted in a blind-coded manner with respect to genotype. Animals were housed with *ad libitum* access to food and water in a colony room kept at 19–22°C and 40–60% humidity, under a 12:12 h light/dark cycle (lights on at 8 am). All procedures were performed in compliance with the NIH Guide for the Care and Use of Laboratory Animals, and approved by the local animal care committee of Universitat de Barcelona following European (2010/63/UE) and Spanish (RD53/2013) regulations for the care and use of laboratory animals.

Post-mortem human brain tissue

Putamen samples from patients with Huntington's disease and control individuals were supplied by the Neurological Tissue Bank of the Biobank-Hospital Clínic-Institut d'Investigacions Biomèdiques August Pi i Sunyer (IDIBAPS; Barcelona, Catalonia) following the guidelines and approval of the local ethics committee (Hospital Clínic of Barcelona's Clinical Research Ethics Committee). Details are provided in Supplementary Table 1.

Protein extraction and western blot analyses

Protein extraction and western blot analysis were performed as described elsewhere (Saavedra *et al.*, 2010). Immunoblots were probed with the antibodies depicted in Supplementary Table 2. After primary antibody incubation, membranes were washed with TBS-T and incubated for 1 h at room temperature with the appropriated horseradish peroxidase-conjugated secondary antibody (1:2000; Promega), and the reaction was visualized with the western blotting luminol reagent (Santa Cruz Biotechnology). Western blot replicates were scanned and quantified using a computer-assisted densitometre (Gel-Pro Analyzer version 4, Media Cybernetics).

eIF4G immunoprecipitation assay

Brain tissue was homogenized using an insulin syringe in ice-cold immunoprecipitation buffer containing: 40 mM Hepes (pH 7.5), 150 mM NaCl, 10 mM sodium pyrophosphate, 10 mM sodium glycerophosphate, 1 mM EDTA, 0.3% 3-[(3-cholamidopropyl) dimethylammonio]-1-propanesulphonate, 1 mM $NaVO_4$, 2.5 mM NaF, 2 mM PMSF and 1:10 000 protease inhibitor cocktail (Sigma-Aldrich). Protein (200 µg) was incubated overnight at 4°C on a rotary mixer with 5 µg of anti-eIF4G antibody (1 µl/50 µg protein; Cell Signaling) or rabbit IgGs (Jackson Immunoresearch) as a negative control. The immune complexes were precipitated overnight at 4°C with the addition of 5% A-Sepharose Cl-4B (Sigma Aldrich). Beads were collected by centrifugation (5 min, 6000 rpm at 4°C) and washed with immunoprecipitation buffer three

[12.7.2019–7:09pm] [1–19] Paper: OP-BRAI190237
SUBJECT CATEGORY: ORIGINAL ARTICLE MANUSCRIPT CATEGORY: ORIGINAL ARTICLE

times and once with wash buffer containing: 50 mM HEPES (pH 75), 40 mM NaCl, 2 mM EDTA. Immunocomplexes were resolved on 12% SDS-PAGE and analysed by western blot.

SUnSET method in brain slices

SUnSET method was carried out as described by Santini *et al.* (2013). This method is based on the ability of puromycin to label the newly synthesized peptides when administrated at low doses. Animals were sacrificed by decapitation and the brain was quickly removed and maintained with oxygenated artificial CSF (in mM: 125 NaCl; 2.5 KCl; 1.2; NaH_2PO_4; 1.2 $MgCl_2$; 2.4 $CaCl_2$; 26 $NaHCO_3$; 11 glucose). Coronal slices (400 µm) were obtained from wild-type and R6/1 mice using a conventional vibratome. Slices containing cortex and striatum were then incubated for 1 h with oxygenated artificial CSF at 37°C and subsequently treated with puromycin (5 µg/ml) for 45 min. The slices were then flash frozen, and the striatum dissected out. Finally, striatal samples were processed for western blot, as described above, using anti-puromycin antibody. Protein synthesis was determined by measuring total lane signal from 250–25 KDa and normalizing against α-tubulin.

Immunofluorescence

Coronal brain sections (30 µm) were obtained and processed as described elsewhere (Rué *et al.*, 2013). Free-floating brain sections were incubated overnight at 4°C with anti-Puromycin (1:500; Merck Millipore), anti-DARPP-32 (1:500; Cell Signaling), anti-NeuN (1:500; Cell Signaling) or anti-GFAP (1:400; Sigma Chemical) antibodies. Nuclei were stained with Hoechst 33258 (1:4000; Invitrogen, prepared in TBS). Sections were then washed in phosphate-buffered saline (PBS) and incubated for 2 h at room temperature with the corresponding fluorescent secondary antibodies: Cy3 anti-rabbit (1:200) and Cy2 anti-mouse (1:200), both from Jackson ImmunoResearch. To count DARPP-32/puromycin positive neurons and to analyse puromycin staining levels, immunostained sections were examined by using the Leica TCS SP5 laser scanning confocal microscope (Leica Microsystems) with Argon and HeNe lasers coupled to a Leica DMI6000 inverted microscope at 40× magnification. Confocal images were taken as stacks differing in 0.29 µm in Z axis with an HCX PL APO lambda blue 40× numerical aperture objective and standard pinhole (1 Airy disk). For image measurements, 3D Objects Counter plugin in ImageJ software (NIH, Bethesda, MD, USA) was used.

Immunohistochemistry

Coronal sections (30 µm) of the whole brain were obtained. Anti-EM48 (1:150; Millipore) antibody was used to detect mhtt aggregates in free-floating brain slices as described elsewhere (Giralt *et al.*, 2011). Briefly, sections were incubated with biotinylated secondary antibody (1:200; Thermo Fisher) and developed with diaminobenzidine (DAB). EM48 staining was examined and photographed at 40× using Computer-Assisted Stereology Toolbox (CAST) software (Olympus Denmark A/S). All images were analysed using CellProfiler Analyst software (Jones *et al.*, 2008).

PUNCH-P

PUNCH-P was performed as described elsewhere (Aviner *et al.*, 2014). Briefly, pools of three whole brains from 15-week-old wild-type and R6/1 mice were used to isolate active ribosomes with ice-cold polysome buffer: 50 mM Tris-HCl (pH 7.5), 10 mM MgCl2 and 25 mM KCl, EDTA-free complete protease inhibitor mix, 1.4 µg/ml pepstatin, 2 µg/ml leupeptin and 40 U/ml RNasin. After tissue homogenization with glass tissue grinder, the volume of the cell suspension was measured, and one-tenth volume of ice-cold lysis buffer was added [11% (w/v) sodium deoxycholate (Sigma Chemical Co) and 11% (v/v) Triton X-100 (Merck Millipore) in polysome buffer]. After 20 min incubation of the lysate with the lysis buffer, it was clarified by centrifugation at 20 000 *g* for 10 min at 4°C. The ribosomes were isolated by centrifugation at 48 600 *g* using a sucrose solution. The concentration of ribosomes was determined by measuring rRNA absorbance at 254 nm with a spectrophotometer. We first adjusted the concentration of bio-puromycin and the amount of resin necessary for the proper isolation of newly synthesized peptides (Supplementary Fig. 1). Biotin-puromycin was added (100 pmol per 1 OD254 units of ribosome-containing solution) and the mix was incubated at 37°C for 15 min. The newly synthesized polypeptides were captured overnight, at room temperature, by adding 5 µl streptavidin bead slurry per 1 OD254 units of ribosome. The day after, the polypeptides were washed with different buffers (urea/SDS buffer, 1 M NaCl, double-distilled water, 1 mM DTT, 50 mM iodoacetamide, 50 mM ammonium bicarbonate) to finally digest the polypeptides with trypsin and perform liquid chromatography-tandem mass spectrometry analysis in collaboration with 'Unitat de Proteòmica' from the University of Barcelona, Barcelona, Spain.

Acute intracerebroventricular puromycin infusion

Fifteen-week-old wild-type and R6/1 mice were deeply anaesthetized with a mixture of oxygen and isoflurane (5% induction and 1% maintenance) and placed in a stereotaxic apparatus for intracerebroventricular injection (coordinates: −0.22 mm anterio-posterior, +1 mm mediolateral, and −2.2 mm dorsoventral) of puromycin (3 µl of puromycin solution; 9 mg/ml, 10% DMSO/90% saline), which was infused using a 10 µl-Hamilton microlitre syringe at an infusion rate of 1 µl/min. The needle was left in place for 3 min to ensure a proper diffusion.

Surgery for 4EGI-1 treatment

Cannula implantation and drug treatments were performed as described by Santini *et al.* (2013). Briefly, wild-type and R6/1 mice were placed in the stereotaxic apparatus under isofluorane anaesthesia (5% induction and 1% maintenance), and a guide cannula (26-G, Plastics One Inc) was implanted at the following coordinates from bregma and dura matter: −0.22 mm anteroposterior, +1 mm mediolateral, and −2.4 mm dorsoventral. Mice were recovered from the surgery for 1 week and intracerebroventricular pharmacological treatments were subsequently started. Mice received daily vehicle (artificial CSF) or 4EGI-1 (0.5 µl at 20 µM) for 6 days. Drugs

[12.7.2019–7:09pm] [1–19] Paper: OP-BRAI190237
SUBJECT CATEGORY: ORIGINAL ARTICLE MANUSCRIPT CATEGORY: ORIGINAL ARTICLE

were infused at 0.25 µl/min in awake and freely moving mice. After infusion, the cannula was left for an additional 3 min to ensure a proper diffusion of the drug and avoid reflux. On the last day of infusions, mice received vehicle or 4EGI-1 plus puromycin (25 µg in 0.5 µl) in parallel. Behavioural analysis and tissue dissection were carried out 1 h after 4EGI-1 infusions.

Behavioural assessment

Open field

Open field consisted of a white square arena (40 × 40 cm) and 40 cm high with opaque white walls without external cues. The light intensity was 20 lux throughout the arena. Mice were placed in the centre of the arena and allowed to move freely for 10 min while being tracked with SMART Junior Software. The surface of the arena was rigorously cleaned with 10% ethanol to avoid odours before each trial. For analysis, the arena was divided into a central and a peripheral zone, representing this last a quarter of the first. Distance travelled, and time expended in both zones were recorded. Finally, defecations in the open field were counted manually.

Accelerating rotarod

With neither training nor habituation sessions, mice were placed on a motorized rod (30 mm diameter) with gradual speed increase from 4 to 40 rpm over 5 min, and the latency to fall when the animal was unable to keep up with the increasing speed was recorded. Only the trials where the mice put all four paws on the rod were considered valid and subsequently evaluated. The test was performed three times per day, with an intertrial interval of 1 h, over three consecutive days

Balance beam

Mice were placed on a 50 cm long wooden square prism with 1.3 cm face, and their ability to transverse it was evaluated. The beam was placed horizontally, 40 cm above the bench surface, and divided into 5 cm frames. The test consisted of two sessions, the training and the testing, separated by 4 h. Animals were allowed to walk for 2 min along the beam, and the number of slips and the distance covered were measured in both sessions. Only data from the testing session are represented in the figures.

Vertical pole

Mice were placed just below the top of a vertical pole facing upwards. The wooden pole was wrapped in tape to facilitate walking. Mice were trained over two consecutive days and testing was performed on the third day (three trials per session). Both the time to complete a turn and the time to climb down the pole, were measured. Trials in which the mouse fell from the pole were counted. Trials in which mice descended the pole without complete reorientation were counted as error trials and analysed separately.

Electrophysiology

Surgery

Animals were anaesthetized with 0.8–3% isoflurane delivered from a calibrated Fluotec 5 (Fluotec-Ohmeda) vaporizer at a flow rate of 1 l/min oxygen. A first batch of animals (R6/1 = 9; wild-type = 17) was implanted with two recording electrodes at the right striatum (0.14 mm anterior to bregma, 2.2 mm lateral from midline and 3 mm depth from brain surface) and two bipolar stimulating electrodes at the ipsilateral M2 area of the motor cortex (2.46 mm anterior to bregma, 1 mm lateral from midline and 0.8 mm depth from brain surface). Stereotaxic coordinates were selected following a recent precise description of motor cortex projections to the caudate/putamen complex in mice (Hintiryan *et al.*, 2016). Electrodes were made of 50 µm Teflon-coated tungsten wire (Advent Research Materials Ltd). The final location of the recording electrode was determined using as a guide, the field potential depth profile evoked by paired (40 ms of interval) pulses presented at the M2 area. Two bare silver wires (0.1 mm in diameter) were affixed to the skull as ground. The six wires were connected to a four-pin socket that was fixed to the skull with the help of two small screws and dental cement (Gruart *et al.*, 2006). For a second experiment, animals (R6/1 = 40; wild-type = 32) were also chronically implanted with a blunted, stainless steel guide 26-G cannula (Plastic One) in the lateral ventricle contralateral to the implanted electrodes (0.5 mm posterior to bregma, 1 mm lateral, and 1.8 mm from the brain surface). The tip of the cannula was aimed to be in the centre of the ventricle. Guide cannulas were anchored to the skull by dental cement. After completing surgery stainless steel stylets were inserted into the guide cannula and left in place until injections were made.

Input/output curves, paired pulse facilitation and long-term depression in behaving mice

For input/output curves, mice were stimulated at the motor cortex with single positive-negative pulses at increasing intensities (0.02–0.4 mA). The effects of paired pulses at different interpulse intervals (20, 40, 100, 200, and 500 ms) were also checked. We used intensities corresponding to ~40% of the amount necessary to evoke a saturating response. In all the cases, the pair of pulses of a given intensity was repeated × 10 times with time intervals × 30 s, to avoid as much as possible interferences with slower short-term potentiation (augmentation) or depression processes. Moreover, to avoid any cumulative effect, intensities and intervals were presented at random (Madronal *et al.*, 2009).

For evoking long-term depression (LTD) in behaving mice, we followed procedures described previously (Gruart *et al.*, 2006). Field potential baseline values were collected 15 min prior to LTD induction using single 100 µs, square, biphasic pulses. Pulse intensity was set at ~40% of the amount necessary to evoke a maximum field potential response (0.15–0.25 mA)—i.e. well below the threshold for evoking a population spike. For LTD induction, animals were presented with a low frequency stimulation (LFS) protocol consisting of a train of 600 pulses at 1 Hz, lasting for 10 min (Berger *et al.*, 2017). In some preliminary experiments carried out in wild-type mice, we confirmed that this LFS protocol evoked larger and longer-lasting LTD than classically used high-frequency stimulation

[12.7.2019–7:09pm] [1–19] Paper: OP-BRAI190237
SUBJECT CATEGORY: ORIGINAL ARTICLE MANUSCRIPT CATEGORY: ORIGINAL ARTICLE

procedures (Dang *et al.*, 2012; Jurado-Parras *et al.*, 2012; Braz *et al.*, 2017). To avoid evoking large population spikes and/or the appearance of cortical seizures, the stimulus intensity during LFS was set at the same value as used for generating baseline recordings. After the LFS session, the same single stimuli were presented every 20 s for 60 min more and for 30 min the following 3 days.

In a second series of experiments, animals were administered with vehicle or 4EGI-1, as described above. Injections took place 45 min before presenting the LFS protocol.

Histology

Once experiments were finished, mice were deeply re-anaesthetized (sodium pentobarbital, 50 mg/kg) and perfused transcardially with saline and 4% phosphate-buffered PFA. Their brains were removed, post-fixed overnight at 4°C, and cryoprotected in 30% sucrose in PBS. Sections (50 µm) were obtained in a microtome (Leica) and those including the cortex and striatum were mounted on gelatinized glass slides and stained with 0.1% toluidine blue to determine the location of stimulating and recording electrodes and of the implanted cannula.

Electrophysiological data collection and analysis

Field potentials evoked at the striatum and 1 −V rectangular pulses corresponding to cortical stimulation were stored digitally on a computer through an analogue/digital converter (CED 1401 Plus). Data were analysed off-line for quantification of field potential recordings with the Spike 2 program (CED). The slope of evoked striatal field responses was computed as the first derivative (V/s) of collected recordings (V). A minimum of five successive field potential responses were averaged, and the mean value of the slope during the rise-time period (i.e. the period of the slope between the initial 10% and the final 10% of the recorded field potential) was determined. Computed results were processed for statistical analysis using the IBM SPSS Statistics 18.0 (IBM, Armonk, New York, USA).

Measurement of ATP levels

Striatal frozen tissue obtained 1 h after the last infusion of vehicle or 4EGI-1 was used to measure ATP levels using the ATP Assay Fluorometric Kit (ab83355; Abcam) according to the manufacturer's instructions. Briefly, striatal tissue was homogenized with ATP assay buffer with a dounce homogenizer. After the removal of insoluble material by centrifugation, proteins were removed from the supernatant with perchloric acid. Then, in a 96-well plate, standard and sample wells were prepared following the instructions. Finally, the ATP reaction mix was added into each well to finally measure on a microplate reader at OD 570 nm. The experiment was performed in duplicate.

Ribosome visualization

Animals were perfused and brains processed as described above. Coronal sections (30 µm) fixed on coated slides were treated with PBS plus 0.1% Triton X-100 for 10 min. After washing twice with PBS for 5 min, slices were stained with NeuroTrace 500/525 Green Fluorescent Nissl Stain (N21480; 1:200; Invitrogen) for 20 min at room temperature. Finally, brain slices were washed for 2 h at room temperature in PBS and covered with a coverslip using Mowiol-mounting media (Merck). Six to eight striatal sections for animal were analysed. Signal intensity from the striatum was quantified using the Cell Profiler software 3.0.0.

Statistical analysis

In most of the graphs, each point represents data from an individual mouse All the results were expressed as the mean ± standard error of the mean (SEM). Statistical analysis was performed using the Student's *t*-test or the two-way ANOVA, followed by a *post hoc* test as appropriate and indicated in the figure legends. A 95% confidence interval was used and values of $P < 0.05$ were considered as statistically significant.

Data availability

The raw data that support the findings of this study are available from the corresponding author upon reasonable request. AQ3

Results

4E-BP1 is inactivated in the Huntington's disease striatum

To investigate the phosphorylation status of 4E-BP in cells expressing mHtt, we analysed by western blot the levels of total and phosphorylated form of 4E-BP at Thr37/46 (p4E-BP) in the striatum of R6/1, R6/2 and Hdh$^{Q7/Q111}$ knock-in (KI) mice, in the putamen of patients with Huntington's disease, and in their respective controls. Western blot analysis revealed increased p4E-BP and decreased 4E-BP levels in the striatum of R6/1 mice from early stages of disease in comparison with wild-type mice (Fig. 1A). Similarly, KI mice showed increased striatal levels of p4E-BP from 13 months of age and onwards (Fig. 1B), but total 4E-BP levels were not altered in comparison with wild-type animals. Moreover, we detected increased p4E-BP and decreased 4E-BP levels in the striatum of R6/2 mice at 12 weeks of age (Fig. 1C). In agreement with the results obtained in R6 mice striatums, 4E-BP total levels were decreased in the putamen of Huntington's disease patients compared with non-affected individuals (Fig. 1D). Unfortunately, we could not detect any phosphorylated form of 4E-BP in human brain samples. AQ4 AQ5

Protein translation is increased in the striatum of Huntington's disease mouse models

Our results showed that 4E-BP was hyper-phosphorylated and subsequently inactivated in the striatum of Huntington's disease mouse models. If the 4E-BP–eIF4E interaction is reduced, then the eIF4F (eIF4E-eIF4G) complex is expected to be increased and cap-dependent translation overactivated. Thus, we evaluated the interaction between eIF4E and eIF4G in the striatum of wild-type and R6/1

[12.7.2019–7:09pm] [1–19] Paper: OP-BRAI190237
SUBJECT CATEGORY: ORIGINAL ARTICLE MANUSCRIPT CATEGORY: ORIGINAL ARTICLE

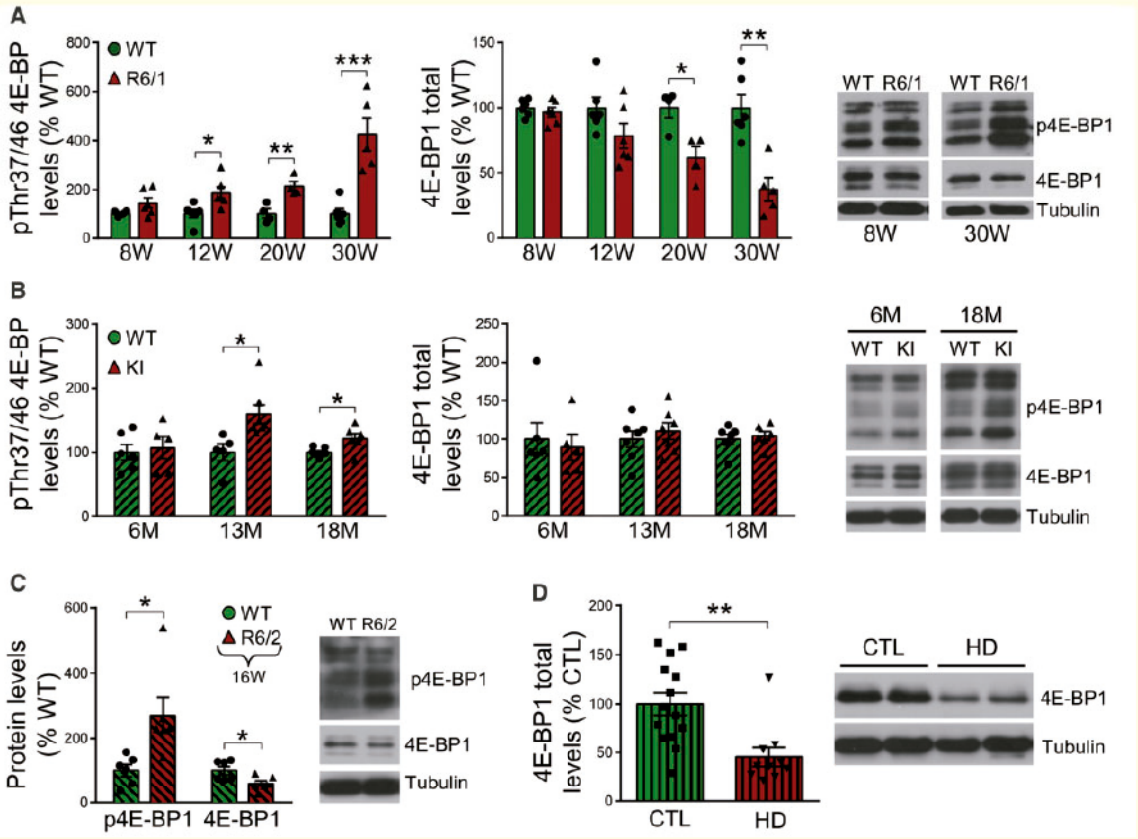

Figure 1 4E-BP is inactivated in the striatum of Huntington's disease. (**A–C**) Quantification (*left*) and representative immunoblots of striatal lysates (*right*) of phosphorylated and total levels of 4E-BP at different stages of the disease progression (W = weeks; M = months) in (**A**) R6/1, (**B**) $Hdh^{Q7/Q111}$ (KI) and (**C**) R6/2 mice, and their corresponding wild-type (WT) littermates. Tubulin was used as loading control. Data are expressed as a percentage of wild-type mice. Each point corresponds to the value from an individual mouse. Bars represent the mean ± SEM. Two-tailed unpaired *t*-test, ***$P < 0.001$, **$P < 0.01$, *$P < 0.05$. (**D**) Total levels of 4E-BP in the putamen of non-affected individuals (CTL) and Huntington's disease (HD) patients. Tubulin was used as loading control. Data are presented in percentage relative to control subjects. Each point corresponds to the value from an individual subject, and bars represent the mean ± SEM. Two-tailed unpaired *t*-test, **$P < 0.01$.

mice by co-immunoprecipitation. Immunoprecipitation of eIF4G and posterior quantitative western blotting revealed increased interaction between eIF4G and eIF4E in the striatum of R6/1 mice (Fig. 2A), while no changes in total levels of eIF4F complex forming proteins were detected (Supplementary Fig. 2). To test if this increased interaction results in increased translation, we applied the SUnSET method. In brain slices containing the corticostriatal pathway obtained from 15-week-old R6/1 and 13-month-old KI mice, we found an increase in the incorporation of puromycin by striatal cells when compared with their corresponding wild-type littermates (Fig. 2B and C). In striatal samples from the same R6/1 mice used to analyse puromycin incorporation, we measured p4E-BP protein levels (Fig. 2D) and observed a good correlation between the increase in *de novo* cap-dependent translation and 4E-BP1 inactivation (Fig. 2E). Importantly, we observed that increased translation in R6/1 mouse striatum occurred mainly in DARPP-32 positive neurons (Fig. 2F), while GFAP positive cells did not co-localize with puromycin (Supplementary Fig. 3). The percentage of DARPP-32 positive neurons showing puromycin staining was similar in wild-type and R6/1 mice striatums (Fig. 2F), but striatal DARPP-32 positive cells from R6/1 mice showed increased puromycin intensity (Fig. 2F).

Increased translation in Huntington's disease striatum affects proteins from selective pathways

To identify the proteins that are being newly synthesized in R6/1 in comparison with wild-type mice striatums, we used the PUNCH-P approach (Aviner *et al.*, 2014), which was applied in 15-week-old wild-type and R6/1 mice whole

[12.7.2019–7:09pm] [1–19] Paper: OP-BRAI190237
SUBJECT CATEGORY: ORIGINAL ARTICLE MANUSCRIPT CATEGORY: ORIGINAL ARTICLE

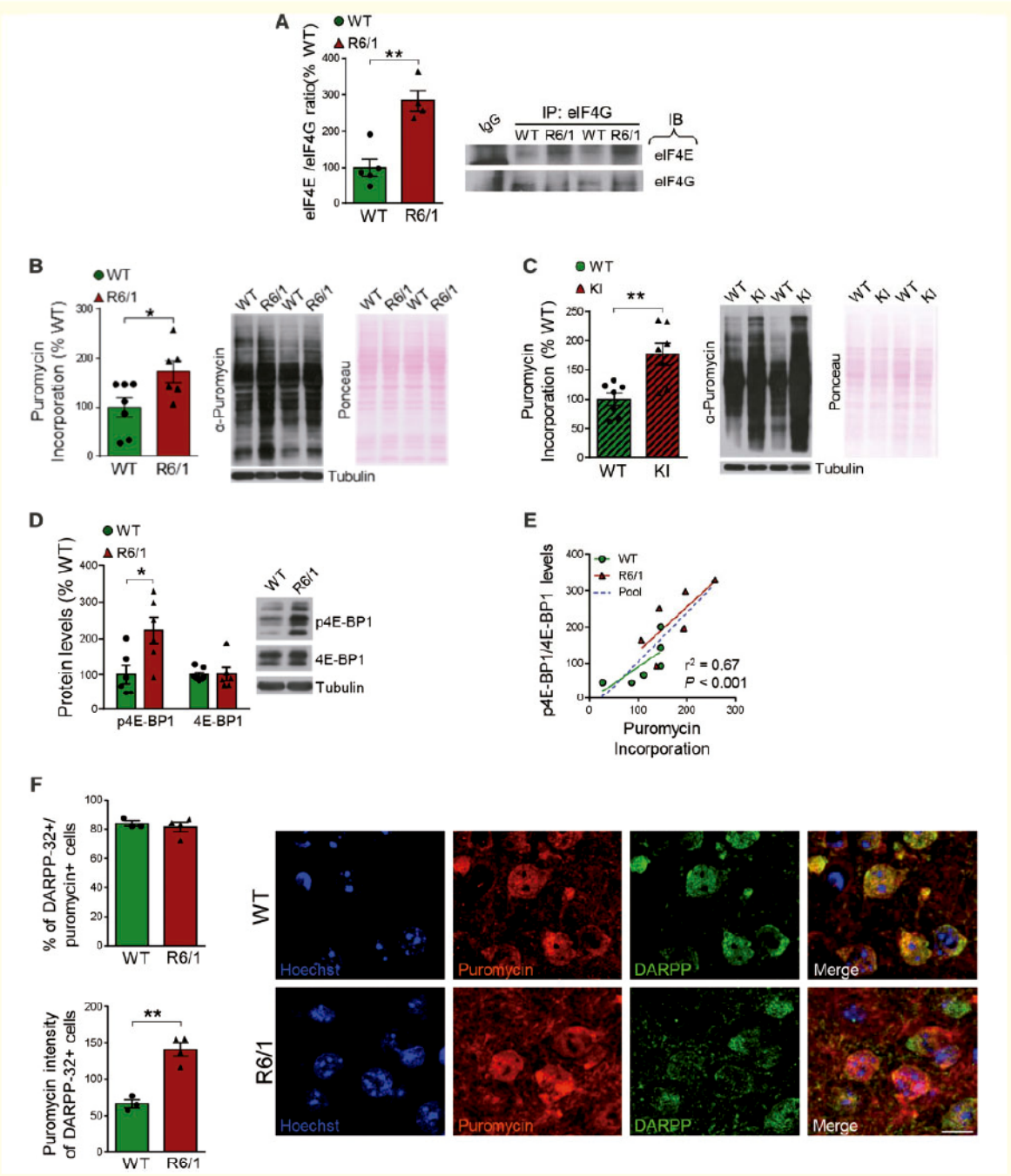

Figure 2 Increased levels of the eIF4F complex and translation in the R6/1 mice striatums. (**A**) Co-immunoprecipitation analysis of eIF4E and eIF4G in striatal lysates from 20-week-old wild-type (WT) and R6/1 mice. Quantification of eIF4E levels relative to immunoprecipitated eIF4G. Values are shown as the mean ± SEM, $n = 4$–5 mice per genotype. Two-tailed unpaired *t*-test, $^{**}P < 0.01$. Quantification (*left*) and representative immunoblot (*right*) of striatal lysates obtained from brain slices (containing the cortex and striatum) from 15-week-old wild-type and R6/1 (**B**) and 13-month-old wild-type and $Hdh^{Q7/Q111}$ (KI) mice (**C**) incubated with puromycin to measure basal rates of protein synthesis. α-Tubulin and Ponceau S staining were used as loading controls. Puromycin incorporation is presented as the percentage change relative to vehicle-treated wild-type slices and normalized against α-Tubulin. Mean ± SEM, $n = 6$–7 mice per genotype. Two-tailed unpaired *t*-test, $^{*}P < 0.05$; $^{**}P < 0.01$. (**D**) Quantification (*left*) and representative immunoblot (*right*) of phosphorylated and total 4E-BP analysed in the same striatal samples where protein synthesis was analysed. Mean ± SEM, $n = 6$–7 mice per genotype Two-tailed unpaired *t*-test, $^{*}P < 0.05$. (**E**) Correlation between

(continued)

[12.7.2019–7:09pm] [1–19] Paper: OP-BRAI190237
SUBJECT CATEGORY: ORIGINAL ARTICLE MANUSCRIPT CATEGORY: ORIGINAL ARTICLE

Table 1 Biological process related to the differently expressed proteins

Biological process	Stat. mean	Set. size	P_{up}	P_{dn}	*P*-value	q-value
Ribosome	3.02359	23	0.00251	0.99749	0.00502	0.02132
Oxidative phosphorylation	2.78810	14	0.00756	0.99244	0.01512	0.02367
Phagosome	2.30952	10	0.02284	0.97716	0.04567	0.04982
Dopaminergic synapse	-2.92431	14	0.99633	0.00367	0.00734	0.02132
Neurotrophin signalling pathway	-2.92760	10	0.99467	0.00533	0.01066	0.02132
TNF signalling pathway	-2.92976	10	0.9947	0.0053	0.01061	0.02132
Retrograde endocannabinoid signalling	-3.08791	11	0.99665	0.00335	0.00671	0.02132

Pathway enrichment analysis was performed on the Pathview web platform that uses the KEGG pathway database. Stat. mean = mean of gene set test statistics; Set. size = the effective gene set size, i.e. the number of genes included in the gene set test; P_{up} = *P*-value for over-representation of the GO term in the upregulated genes; P_{dn} = *P*-value for over-representation of the GO term in downregulated genes; *P*-value = global *P*-value or summary of the individual *P*-values from multiple single array; based gene set tests. This is the default *P*-value being used; q-value = FDR q-value adjustment of the global *P*-value using the Benjamini and Hochberg procedure implemented in multi-test package. This is the default q-value being used.

brains (Fig. 3A). We identified ~1400 proteins in each pool of animals per genotype (Fig. 3B). The summation of identified peptide sequences (peptide spectrum matches, PSMs) for proteins tend to increase, although it did not reach statistical significance, in R6/1 mice brains (Fig. 3C). This parameter was considered a quantitative measurement of the amount of detected proteins. Next, we identified 233 proteins differently expressed (146 up- and 87 down-translated) between genotypes (Fig. 3D and Supplementary Table 3). We used the SPIA analysis method to identify the possible pathways selectively affected by the differently translated peptides. Interestingly, we detected that in R6/1 mice brains, some proteins were increased while others were decreased. Proteins related with ribosomes and oxidative phosphorylation were among the proteins increased (Table 1 and Fig. 3E) with components of complex I of the respiratory chain as the most affected, but also proteins related with ubiquinol-cytochrome C reductase complex (complex III or cytochrome b-c1 complex) and ATP V-type ATPase were increased (Supplementary Table 3). On the other hand, structural and functional neuronal-related proteins, such as proteins from the dopaminergic synapse and the endocannabinoid signalling, were decreased (Fig. 3E).

Treatment with 4EGI-1 improves motor function in Huntington's disease mice

Considering that increased protein synthesis could lead to neuronal dysfunction in Huntington's disease striatum, we took advantage of 4EGI-1, an inhibitor of eIF4G-eIF4E interaction (Moerke *et al.*, 2007), in order to normalize protein synthesis. An infusion cannula was implanted in the lateral ventricle of 13-week-old wild-type and R6/1 mice and 1 week after the surgery, vehicle or 4EGI-1 (20 μM, a dose known to not modulate behaviour in wild-type mice; Santini *et al.*, 2013) were infused daily for 6 days (Fig. 4A). Motor behaviour was tested by using the open field, the accelerating rotarod test, the vertical pole task and the balance beam test. Interestingly, 4EGI-1 administration improved motor behaviour in R6/1 mice, as shown in all the tests analysed whereas it did not produce any effect in wild-type mice (Fig. 4B–E). Furthermore, 4EGI-1 did not alter spontaneous locomotor activity, anxious behaviour or body weight in both wild-type and R6/1 mice (Supplementary Fig. 4).

Treatment with 4EGI-1 normalizes protein synthesis in R6/1 striatum

On the last day of treatment with 4EGI-1, puromycin was co-infused together with vehicle or 4EGI-1 in wild-type and R6/1 mice. One hour later, mice were sacrificed, and protein synthesis evaluated in the striatum. As in naïve mice (Fig. 2B), we detected increased translation and eIF4G-eIF4E interaction in vehicle-treated R6/1 mice striatums that were normalized to wild-type levels after 4EGI-1 treatment (Fig. 5A and B).

The PUNCH-P experiment revealed increased synthesis of ribosomal proteins in R6/1 mice brains (Fig. 3), suggesting that ribosome content could be increased in the

Figure 2 Continued
p4E-BP/4E-BP levels and puromycin incorporation in wild-type, R6/1 mice ($n = 7$ wild-type; 6 R6/1), and in the pool (WT + R6/1 mice) as determined by simple linear regression. **(F)** Quantitative analysis of (i) the percentage of striatal DARPP-32 positive neurons showing puromycin staining; and (ii) puromycin intensity in striatal DARPP-32 positive neurons. Mean ± SEM, $n = 3$–4 mice per genotype Two-tailed unpaired *t*-test, $^{**}P < 0.01$. Representative images showing puromycin and DARPP-32 immunostaining in the striatum of 15-week-old R6/1 mice, 45 min after the infusion puromycin [3 μl of puromycin solution (9 mg/ml, 10% DMSO/90% saline)] in the lateral ventricle. *Right* image shows the co-localization between puromycin and DARPP-32. Scale bar = 10 μm. IB = .

AQ11

[12.7.2019–7:09pm] [1–19] Paper: OP-BRAI190237
SUBJECT CATEGORY: ORIGINAL ARTICLE MANUSCRIPT CATEGORY: ORIGINAL ARTICLE

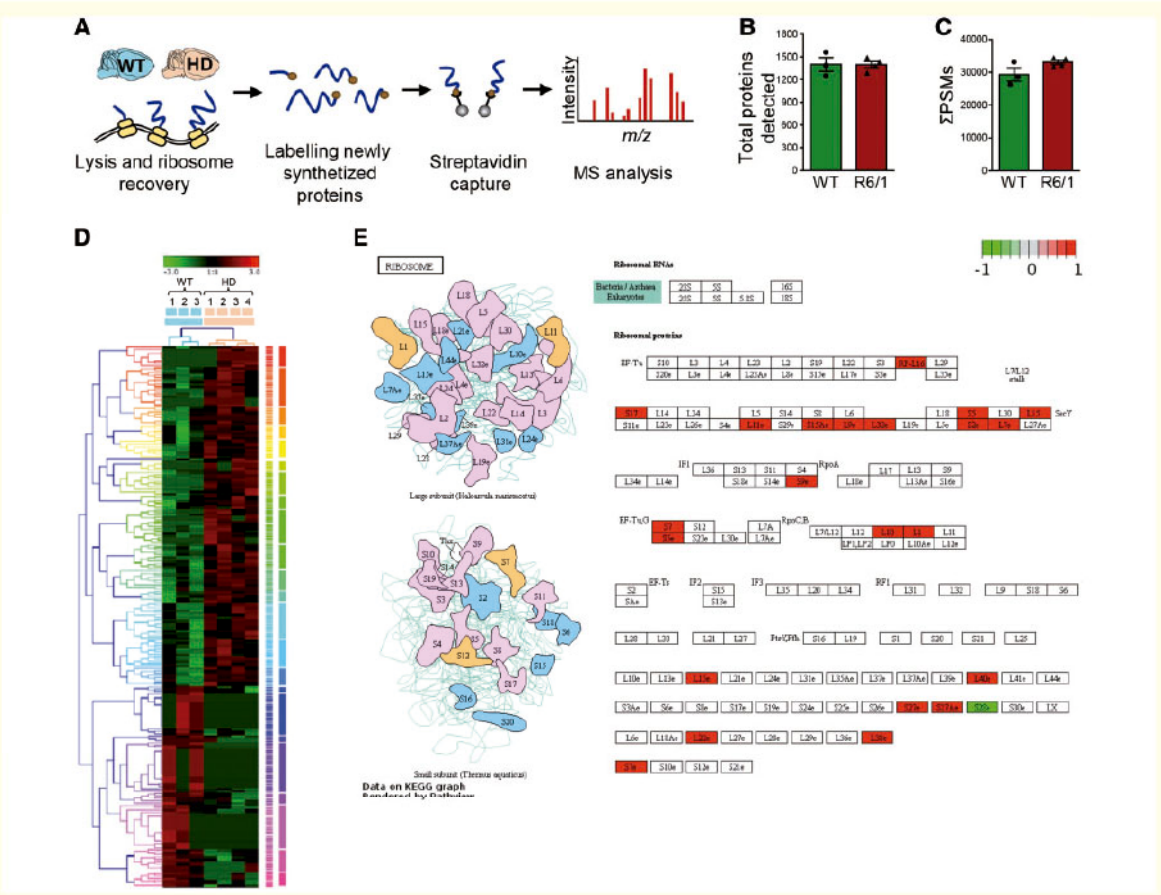

Figure 3 PUNCH-P method revealed selective differences in R6/1 mice translatome. (**A**) Scheme showing the PUNCH-P protocol. Newly synthesized peptides were isolated and identified in pools of three 15-week-old wild-type (WT, $n = 3$) and R6/1 (HD, $n = 4$) mice brains each. (**B**) Total number of detected proteins/pool. Mean ± SEM. (**C**) Summation of peptide spectrum matches (PSMs) shows a slight increase in R6/1 mice. Mean ± SEM. (**D**) Heat map representation of 233 differentially expressed proteins. (**E**) KEGG graph generated by Pathview showing the ribosomal proteins significantly increased in R6/1 mice. MS=.

AQ12

striatum. To examine this possibility, we used the fluorescent dye NeuroTrace Green, which labels neuronal ribosomes (Slomnicki *et al.*, 2016), and analysed by western blot ribosomal proteins, RPL10, RPS27A and S7, that were detected as up-synthesized in the R6/1 mice brains by the PUNCH-P experiment. Ribosome content (Fig. 5C and D), RPS27A and S7 (Fig. 5F and G), but not RPL10 (Fig. 5E) protein levels were increased in the striatum of vehicle-treated R6/1 compared with vehicle-treated wild-type mice. Interestingly, 4EGI-1 treatment normalized ribosomal content in R6/1 mice with no effects in the striatums of wild-type mice (Fig. 5C). RPL10, RPS27A and S7 protein levels in 4EGI-1-treated R6/1 mice striatums did not differ from levels in wild-type mice striatums (Fig. 5E–G). Similarly, we detected increased levels of cyclin D1, a protein previously shown to increase when 4E-BP is inactivated (Rosenwald *et al.*, 1995), in the striatum of vehicle-treated R6/1 mice whose levels were normalized by 4EGI-1 treatment (Supplementary Fig. 5A). In addition, we analysed the levels of striatal proteins DARPP-32 (Bibb *et al.*, 2000; van Dellen *et al.*, 2000) and STEP46 (Luthi-Carter *et al.*, 2000; Desplats *et al.*, 2006; Saavedra *et al.*, 2011) that are decreased in the Huntington's disease striatum, and of soluble and insoluble forms of mHtt, which has been suggested as a cap-dependent translated protein (King *et al.*, 2008). Treatment with 4EGI-1 was unable to restore DARPP-32 and STEP46 (Supplementary Fig. 5A and B) protein levels, nor to reduce the levels of soluble and insoluble mHtt and the number of mHtt aggregates (Supplementary Fig. 6) in R6/1 mouse striatum.

Overall, our results show that that 4EGI-1 treatment could be effective in the normalization of aberrant synthesized proteins in Huntington's disease striatum.

[12.7.2019–7:09pm] [1–19] Paper: OP-BRAI190237
SUBJECT CATEGORY: ORIGINAL ARTICLE MANUSCRIPT CATEGORY: ORIGINAL ARTICLE

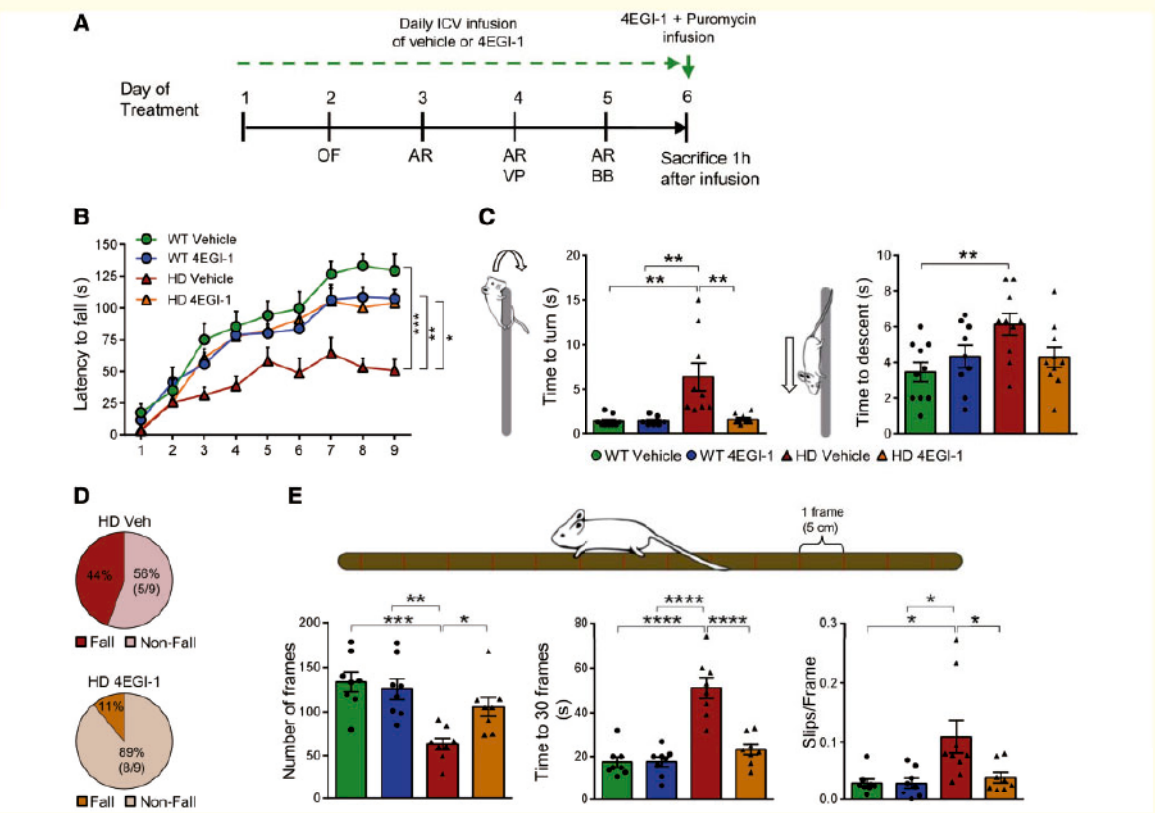

Figure 4 4EGI-1 treatment improves R6/1 mice motor phenotype. (**A**) Schematic representation of the experimental design performed. 4EGI-1 (20 µm) was infused in the lateral ventricle of 15-week-old wild-type (WT) and R6/1 (HD) mice over 6 days. Each test was conducted on the indicated day of treatment. OF = open field; AR = accelerating rotarod test; VP = vertical pole; BB = balance beam. (**B**) Accelerating rotarod test was performed for three consecutive days (three trials per day). The latency to fall per test and group is represented as mean ± SEM (n = 6–8 mice per group). Two-way ANOVA with repeated measures followed by Bonferroni's *post hoc* test, *$P < 0.05$; **$P < 0.01$; ***$P < 0.001$. (**C**) Vertical pole: time to turn (*left*) and time to descent (*right*) was recorded after placing the mice upwards to the pole. Three trials were conducted and data represent the mean ± SEM (n = 8–9 mice per group). Two-way ANOVA followed by Bonferroni's *post hoc* test, **$P < 0.01$. (**D**) Percentage of R6/1 mice that felt from the pole during the Vertical Pole test when trying to turn or descend. No falls were recorded in any wild-type mice. Two-tailed unpaired *t*-test, ****$P < 0.0001$. (**E**) Balance beam: from *left* to *right*; number of frames crossed in 2 min, time to cross 30 frames and number of slips committed per frame in 2 min. Data represent the mean ± SEM (n = 8 mice per group). Two-way ANOVA followed by Bonferroni's *post hoc* test, *$P < 0.05$; **$P < 0.01$; ***$P < 0.001$, ****$P < 0.0001$. ICV =.

AQ13

Normalization of protein synthesis partially improves long-term depression in R6/1 mice

As alterations in translation have been associated with impaired synaptic plasticity (Santini *et al.*, 2013, 2017), we speculated that increased protein synthesis could be partially responsible for the corticostriatal dysfunction found in Huntington's disease mouse models (Cepeda *et al.*, 2003; Parievsky *et al.*, 2017). Thus, we first evaluated corticostriatal LTD in behaving wild-type and R6/1 mice in basal conditions (Fig. 6; see Fig. 7A for placement of the electrodes). Input/output curves (I/O: as a global measure of synaptic efficacy) and paired-pulse facilitation (PPF; presynaptic function and neuromodulation) were similar in wild-type and R6/1 mice (Fig. 6B and C). To evaluate possible post-synaptic alterations in 15-week-old R6/1 mice we compared corticostriatal field excitatory postsynaptic potentials (fEPSPs) after LFS of the motor (M2) cortex in wild-type and R6/1 mice. Baseline values were collected for 15 min while the animal was stimulated in the M2 area every 20 s. The slopes of evoked field potentials were averaged every 5 min. LTD was evoked by LFS of the motor cortex at 1 Hz for 10 min (given a total of 600 pulses). Wild-type mice presented a significant decrease in the slope of evoked field potentials following the LTD protocol [$F(20,260) = 1.846$; $P = 0.017$] during the first recording session. In contrast, R6/1 mice did not

[12.7.2019–7:09pm] [1–19] Paper: OP-BRAI190237
SUBJECT CATEGORY: ORIGINAL ARTICLE MANUSCRIPT CATEGORY: ORIGINAL ARTICLE

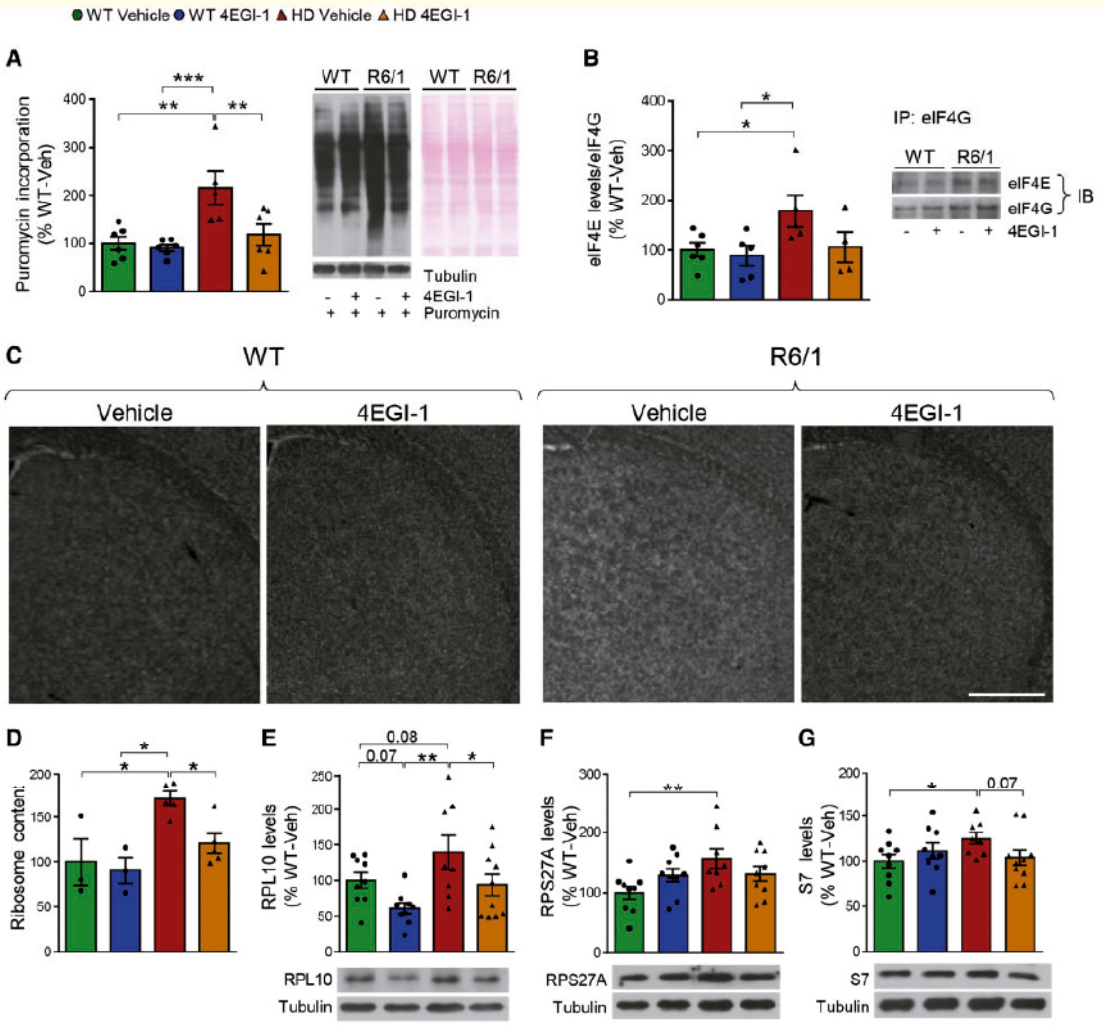

Figure 5 4EGI-1 treatment normalizes translation and recovers ribosomal content in R6/1 mice striatums. (**A**) Quantification of incorporated puromycin (*left*) and representative immunoblot (*right*) of striatal lysates from 15-week-old wild-type (WT) and R6/1 (HD) mice infused over 6 days with vehicle (Veh) or 4EGI-1. Puromycin was co-administered with 4EGI-1 at the last day of treatment and the striatum was dissected out 1 h after. α-Tubulin and Ponceau S staining were used as loading controls. Puromycin incorporation is presented as percentage change relative to vehicle-treated wild-type mice after normalization against α-tubulin. Mean ± SEM. $^{*}P < 0.05$, $^{**}P < 0.01$, two-way ANOVA with Bonferroni's *post hoc* test. (**B**) Co-immunoprecipitation analysis of eIF4E and eIF4G in striatal lysates from wild-type and R6/1 mice after 4EGI-1 or vehicle infusions. Mean ± SEM, $n = 5$–6 mice per genotype. (**C**) Representative images showing fluorescent dye NeuroTrace Greeen staining in the striatum of wild-type and R6/1 mice injected with vehicle or 4EGI-1. Scale bar = 200 µm. (**D**) Quantification of ribosomal content in coronal sections from wild-type and R6/1 mice after 4EGI-1 or vehicle infusions. (**E–G**) Quantification and representative immunoblots of ribosomal proteins RPL10 (**E**), RPS27A (**F**) and S7 (**G**) in striatal lysates obtained from 15-week-old wild-type and R6/1 mice after 4EGI-1 or vehicle infusions. Results are expressed as the mean ± SEM. Two-way ANOVA followed by Fisher's LSD test, $^{*}P < 0.05$; $^{**}P < 0.01$.
IP = immunoprecipitation.

present any sign of LTD following the presentation of the LFS session (Fig. 6D). The slope of field potentials evoked in wild-type mice were significantly ($P < 0.05$) reduced in comparison with values collected from the R6/1 group during the first LTD recording session. No LTD was observed during the second recording session in either group (Fig. 6D). To evaluate whether the behavioural improvement observed in 4EGI-1-treated R6/1 mice was paralleled by an improvement of the corticostriatal function, we monitored LTD. For this, 15-week-old wild-type and R6/1 mice were implanted with stimulating electrodes in the right motor cortex (M2 area), with a recording

[12.7.2019–7:09pm] [1–19] Paper: OP-BRAI190237
SUBJECT CATEGORY: ORIGINAL ARTICLE MANUSCRIPT CATEGORY: ORIGINAL ARTICLE

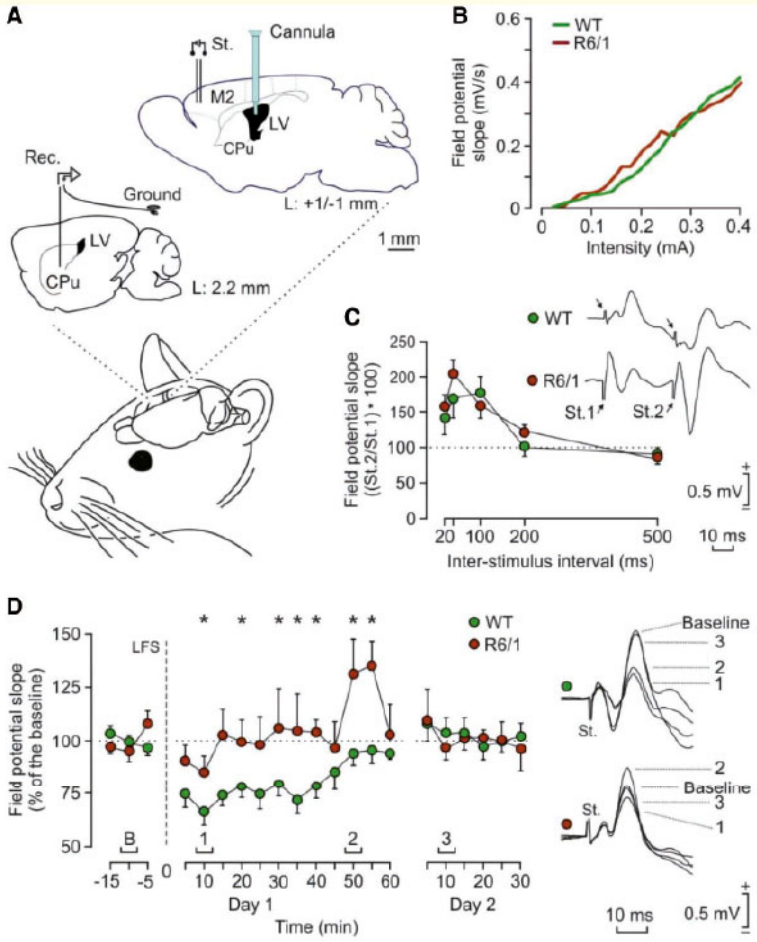

Figure 6 R6/1 mice present similar input/output curves and paired-pulse facilitation, but less LTD, than their wild-type littermates. (**A**) Wild-type and R6/1 mice were chronically implanted with stimulating electrodes in the right motor cortex (M2 area) and with a recording electrode in the ipsilateral striatum. An extra wire was attached to the bone as ground. CPu = caudate-putamen (striatum); LV = lateral ventricle. (**B**) Input/output curves of striatal field potentials evoked by pulses of increasing (0.02–0.4 mA) intensities presented to the ipsilateral M2 area. (**C**) Paired-pulse facilitation in corticostriatal synapses from wild-type and R6/1 mice. The data shown are the mean ± SEM slopes of the second field potential response expressed as a percentage of the first. Selected paired traces (40 ms of inter-pulse interval) collected from representative wild-type and R6/1 mice are illustrated in the *inset*. (**D**) The graph illustrates the time course of LTD evoked at corticostriatal synapses from wild-type and R6/1 mice following an LFS session. The LFS, indicated by the dashed line, was presented after 15 min of baseline recordings. At the right there are illustrated representative examples of field potentials collected at the times indicated below the graph. Field potential slopes are given as a percentage of slope values collected during baseline recordings (100%). $^*P < 0.05$ compared with field potential slopes collected from R6/1 mice (Student's *t*-test).

electrode in the ipsilateral striatum and a cannula in the contralateral ventricle to start infusing 4EGI-1 (0.5 µl at 20 µM) 2 days before LTD induction. The correct locations of stimulating and recording electrodes, and of the implanted cannula, were examined by toluidine blue staining (Fig. 7A). We found that input/output curves evoked in 4EGI-1-treated wild-type mice presented significantly larger [$F(57,304) = 2.609$; $P < 0.001$; two-way repeated measures ANOVA followed by Holm-Sidak multiple comparison procedures] values than wild-type vehicle and the two R6/1 groups, at high (> 0.25 mA) stimulus intensities (Fig. 7B). In contrast, there were no significant differences ($P \geqslant 0.11$) between wild-type vehicle mice and the two R6/1 groups (Fig. 7B). Concerning paired-pulse facilitation, 4EGI-1 injection in wild-type and R6/1 mice 45 min before the test did not modify the effects observed

[12.7.2019–7:09pm] [1–19] Paper: OP-BRAI190237
SUBJECT CATEGORY: ORIGINAL ARTICLE MANUSCRIPT CATEGORY: ORIGINAL ARTICLE

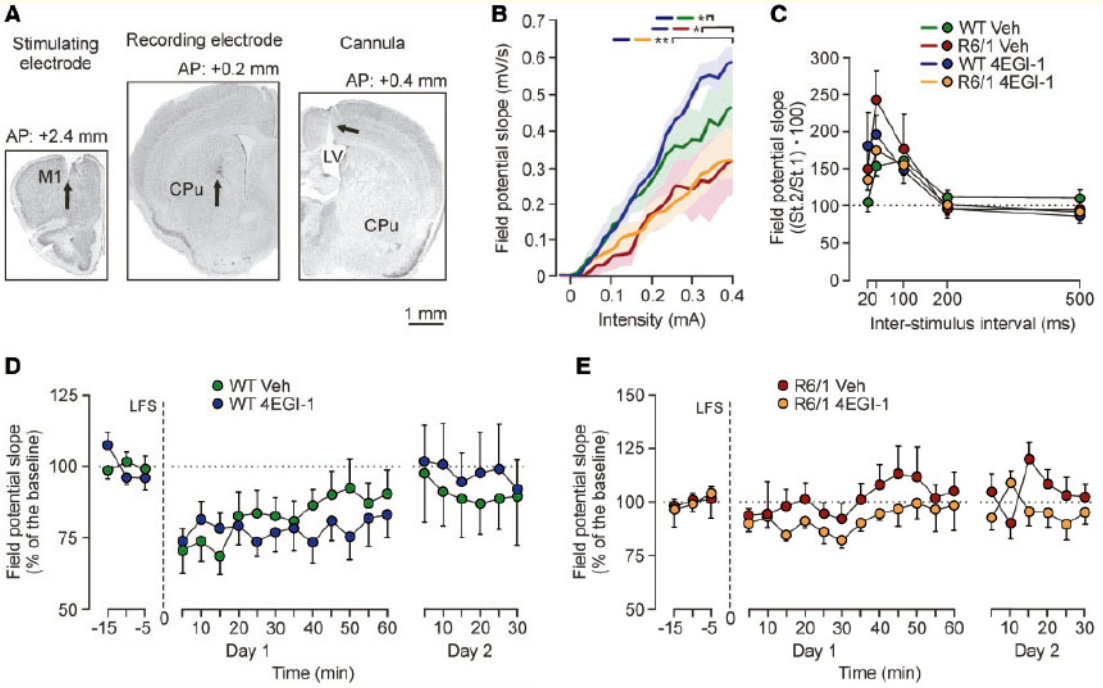

Figure 7 4EGI-1 treatment slightly ameliorates LTD deficits in R6/1 mice. **(A)** Illustrative examples of the location of stimulating and recording electrodes, and of the implanted cannula after toluidine blue staining. CPu = caudate-putamen (striatum); LV = lateral ventricle. **(B)** Input/output curves of striatal field potentials evoked by pulses of increasing intensities presented to the ipsilateral motor cortex (M2) in WT-Veh, WT-4EGI-1, R6/1-vehicle, and R6/1–4EGI-1 groups. Results are expressed as the mean ± SEM. Two-way ANOVA followed by the Holm-Sidak method for multiple comparisons. $*P < 0.05$; $**P < 0.01$. **(C)** Paired-pulse facilitation evoked in cortico-striatal synapses from wild-type and R6/1 mice after infusion of vehicle or 4EGI-1. **(D)** The graph illustrates the time course of LTD evoked at the corticostriatal synapses following an LFS session, indicated by the dashed line, for WT-Veh and WT-4EGI-1 mice. **(E)** The graph illustrates the time course of LTD evoked at the cortico-striatal synapses following an LFS session, indicated by the dashed line, for R6/1-Veh and R6/1–4EGI-1 mice.

in vehicle-injected groups (Fig. 7C). Interestingly, the infusion of 4EGI-1 altered LTD results when compared with vehicle-injected animals. As illustrated in Fig. 7D, although the wild-type vehicle injected group presented a significant ($\chi^2 = 33.322$ with 20 degrees of freedom, $P = 0.031$) LTD in comparison with baseline values, the wild-type 4EGI-1 group presented a longer-lasting LTD ($\chi^2 = 98.330$ with 20 degrees of freedom, $P = 0.001$). Nevertheless, no significant differences were found between the two groups across the sessions [$F(20,240) = 0.264$; $P = 0.999$]. In addition, the intraventricular injection of 4EGI-1 slightly increased the LTD effect in the R6/1 group compared with that evoked in vehicle-treated mice, but without reaching significant values [$F(20,100) = 1.11$; $P = 0.352$] (Fig. 7E). Overall, the local administration of 4EGI-1 did not modify some basic functional properties of striatal neurons as input/output and paired-pulse facilitation in both wild-type and R6/1 mice, but promoted a significant increase in the corticostriatal LTD evoked in wild-type mice, and a non-significant tendency in R6/1 animals.

Discussion

Here, we show that 4E-BP is hypofunctional in Huntington's disease striatum leading to increased formation of the eIF4F complex and, consequently, to exaggerated translation. Increased protein synthesis affects selective pathways including proteins from ribosomes and from the oxidative phosphorylation pathway. Interestingly, pharmacological normalization of protein synthesis in R6/1 mice brains ameliorates motor disturbances and normalizes ribosomal content in the striatum. In addition, we observed a tendency to correct corticostriatal LTD, although it did not reach statistical significance.

Increased p4E-BP and decreased total 4E-BP1 were detected in R6/1 mice striatums from 12 weeks of age onwards. Similarly, 4E-BP levels were reduced in the putamen of Huntington's disease patients. Although mTORC1 has been classically defined as the main kinase phosphorylating 4E-BP at Thr37/46 (Brunn *et al.*, 1997; Gingras *et al.*, 1999), many other kinases have the capability to phosphorylate 4E-BP *in vitro* (Lawrence *et al.*, 1997; Heesom *et al.*,

[12.7.2019–7:09pm] [1–19] Paper: OP-BRAI190237
SUBJECT CATEGORY: ORIGINAL ARTICLE MANUSCRIPT CATEGORY: ORIGINAL ARTICLE

2001; Ito *et al.*, 2016) suggesting that the regulation of 4E-BP phosphorylation is cell type- and physiological context-dependent. The activity of many of these kinases is altered in Huntington's disease striatum such as ERK, p38, PKC or GSK-3β (Bowles and Jones, 2014), and controversial data regarding mTORC1 activity in the striatum of Huntington's disease mouse models has been reported (Ravikumar *et al.*, 2004; Pryor *et al.*, 2014; Lee *et al.*, 2015; Creus-Muncunill *et al.*, 2018). In addition, other mechanisms such as phosphatases (Gardner *et al.*, 2015) and the Rho GTPase RhoE regulate p4E-BP levels (Villalonga *et al.*, 2009). Therefore, the mechanism by which p4E-BP is increased in the presence of mHtt deserves further investigations. Interestingly, 4E-BP dysregulation takes place in brains affected by other neurodegenerative disorders. Alzheimer's disease brains present increased p4E-BP and decreased total levels correlating with tau pathology (Li *et al.*, 2005), and amyloid-β_{1-42} oligomers induce inactivation of 4E-BP (Algarzae *et al.*, 2012; Baleriola *et al.*, 2014). In the same line, different Parkinson's disease causative mutations lead to the inactivation of 4E-BP *in vitro* and *in vivo* (Imai *et al.*, 2008). Thus, our results support the view that altered 4E-BP function could be a common dysregulated mechanism involved in different neurodegenerative disorders.

The inactivation of 4E-BP in R6/1 mice striatums correlated with increased formation of the eIF4F complex and with exaggerated translation, which seems to occur in DARPP-32-positive neurons. Different transcripts can be specifically up-translated when 4E-BP is inactivated (Musa *et al.*, 2016). In fact, the proteomic analysis revealed that ribosomal and oxidative phosphorylation pathway proteins are mainly affected. Increased levels of ribosomal proteins was not fully surprising as inactivation of 4E-BP induces selective enhanced translation of transcripts containing a 5'TOP tract (Jefferies *et al.*, 1994; Avni *et al.*, 1996; Meyuhas, 2000), which encode for components of the translational machinery including ribosomal proteins (Avni *et al.*, 1996; Meyuhas, 2000). Furthermore, 4E-BP has been shown to regulate the translation of mitochondria-related mRNAs (Zid *et al.*, 2009; Goo *et al.*, 2012; Morita *et al.*, 2013) and mRNAs encoding components of mitochondrial ribosomal proteins (also observed in our ribosomal set of proteins) are among them (Morita *et al.*, 2013). On the other hand, previous results have shown complex I defects in patients with Huntington's disease (Parker *et al.*, 1990), but R6/1 mouse striatum showed increased complex I respiration at late stages of disease progression (Herbst and Holloway, 2015) that can be explained by the increase in complex I proteins that we observed. Nonetheless, as previously proposed by others (Herbst and Holloway, 2015), enhanced complex I respiration could be responsible for oxidative stress observed in patients with Huntington's disease (Kumar and Ratan, 2016). Therefore, we could not discard that increased translation of striatal complex I proteins is playing a pathogenic role in Huntington's disease. Taken together, it is tempting to speculate that striatal cells expressing mHtt attempt to compensate the deficit in proteins, such as synaptic proteins, by synthesizing more ribosomes to then increase the global rate of translation (Slomnicki *et al.*, 2016), which is known to be neurotoxic for neurons (Martin *et al.*, 2014*a*). In addition, they activate the synthesis of mitochondrial-related proteins to alleviate energy deficits, which seems insufficient to ameliorate mitochondrial dysfunction occurring in Huntington's disease striatum (Jodeiri Farshbaf and Ghaedi, 2017).

We hypothesized that increased translation in R6/1 mice striatums could be involved in neuronal dysfunction and contribute to motor impairment. Our results support this proposal because infusion of 4EGI-1, an inhibitor of eIF4G-eIF4E interaction (Moerke *et al.*, 2007), normalized protein synthesis and improved motor symptoms. Although the amelioration of motor symptoms did not correlate with a recovery of striatal markers, nor with changes in mHtt levels, 4EGI-1 treatment normalized cyclin D1 levels, previously proposed as a possible contributor to neuronal dysfunction in Huntington's disease (Pelegrí *et al.*, 2008) and re-established ribosomal protein content. Hence, another attractive explanation for the amelioration of motor symptoms is that 4EGI-1 normalization of translation improves protein homeostasis, thereby diminishing energy consumption in striatal cells. Our results also show that the alteration in cortico-striatal LTD detected in R6/1 behaving mice showed a trend toward recovery after 4EGI-1 treatment. The lack of LTD induction observed in R6/1 mice supports the dysfunctional connectivity along the cortico-striatal pathway previously proposed by others (Puigdellívol *et al.*, 2015; Buren *et al.*, 2016; Hintiryan *et al.*, 2016; Rangel-Barajas and Rebec, 2016). Although many studies demonstrated electrophysiological alterations in this pathway (Cepeda *et al.*, 2003; Parievsky *et al.*, 2017), LTD alterations in Huntington's disease were described in hippocampal (Milnerwood *et al.*, 2006) and perirhinal cortex (Cummings *et al.*, 2006) brain slices and our results extend this observation to the cortico-striatal pathway in behaving mice. In agreement with our results, selective mutation in the LRRK2 gene, which induces an enhancement of translation, impairs cortico-striatal LTD in mice (Chou *et al.*, 2014). Overall, our findings are in accordance with previous work reporting that increased protein synthesis is a direct contributor to neuronal dysfunction and behavioural abnormalities that can be tackled pharmacologically with 4EGI-1 treatment (Gkogkas *et al.*, 2013; Santini *et al.*, 2013, 2017; Martin *et al.*, 2014*a*,*b*).

Protein synthesis normalization in Huntington's disease could be achieved in many ways. We speculate that normalization of exaggerated translation might contribute to the beneficial effect of potential Huntington's disease therapies. For instance, Ravikumar *et al.* (2004), showed that the administration of rapamycin to a mouse model of Huntington's disease yielded a dramatic amelioration of motor impairment, accompanied by a reduction in the

[12.7.2019–7:09pm] [1–19] Paper: OP-BRAI190237
SUBJECT CATEGORY: ORIGINAL ARTICLE MANUSCRIPT CATEGORY: ORIGINAL ARTICLE

aggregation of mHtt. From our results and knowing that rapamycin activates 4E-BP (Beretta *et al.*, 1996; Tain *et al.*, 2009), the normalization of protein synthesis could be contributing to rapamycin-mediated neuroprotection in mouse models as has been shown in cellular models of Huntington's disease (King *et al.*, 2008). Interestingly, metformin activation of AMPK has been proposed as a therapeutic strategy for Huntington's disease (Vázquez-Manrique *et al.*, 2015; Jin *et al.*, 2016; Hervás *et al.*, 2017) and AMPK activation inhibits protein synthesis (Chan *et al.*, 2004; Reiter *et al.*, 2008). In addition, among its different mechanisms of action, fingolimod, a drug with beneficial effects in Huntington's disease mouse models (Di Pardo *et al.*, 2014; Miguez *et al.*, 2015), activates PP2A (Yang *et al.*, 2012), a phosphatase that dephosphorylates 4E-BP (Nanahoshi *et al.*, 1998; Nho and Peterson, 2011). Furthermore, prostaglandin E2 EP2 receptor activation has been shown to improve R6/1 phenotype (Anglada-Huguet *et al.*, 2016), which could be attributed to normalization of translation, since prostaglandin E2 suppresses mTOR signalling and inhibits protein synthesis (Okunishi *et al.*, 2014). Finally, 2-methyl-6-(phenylethynyl)pyridine hydrochloride, a drug that has been shown to normalize translation in models of Fragile X Syndrome (Aschrafi *et al.*, 2005; Osterweil *et al.*, 2010), extends lifespan and ameliorates motor disturbances in R6/2 mice (Schiefer *et al.*, 2004). Altogether, this evidence suggests that different therapeutic options proposed for Huntington's disease converge in the normalization of exaggerated protein synthesis.

In conclusion, this study shows increased translation in Huntington's disease striatum affecting the rate of synthesis of selective proteins, such as ribosomes and proteins from the oxidative phosphorylation pathway. Importantly, this aberrant protein synthesis plays a role in motor phenotype associated with Huntington's disease. Therefore, the 4E-BP pathway emerges as a therapeutic target in Huntington's disease.

Acknowledgements

We are very grateful to Ana López and Maite Muñoz for their technical support. We thank Josep Maria Estanyol and Maria José Fidalgo for her critical advice and expertise with PUNCH-P experiment. M. Sánchez Enciso and J.M. González Martín for their help with animal training, and data collection from *in vivo* LTP experiments and their analysis. And thanks to Ana Saavedra and Rafael Alcalá for helpful discussions.

Funding

This work was supported by Ministerio de Economia y Competitividad, Spain (SAF2016–08573-R to EP-N.; BFU2017–82375-R to A.G. and J.M.D-G.; SAF2017–88812R to C.M.) and Fundación Tatiana Pérez de Guzmán el Bueno to A.G. and J.M.D-G. AQ6

Competing interests

The authors report no competing interests.

Supplementary material

Supplementary material is available at *Brain* online.

References

Algarzae N, Hebron M, Miessau M, Moussa CE. Parkin prevents cortical atrophy and Ab-induced alterations of brain metabolism: 13C NMR and magnetic resonance imaging studies in AD models. Neuroscience 2012; 225: 22–34.

Anglada-Huguet M, Vidal-Sancho L, Giralt A, García-Díaz Barriga G, Xifró X, Alberch, J. Prostaglandin E2 EP2 activation reduces memory decline in R6/1 mouse model of Huntington's disease by the induction of BDNF-dependent synaptic plasticity. Neurobiol Dis 2016; 95: 22–34.

Aschrafi A, Cunningham BA, Edelman GM, Vanderklish PW. The fragile X mental retardation protein and group I metabotropic glutamate receptors regulate levels of mRNA granules in brain. Proc Natl Acad Sci USA 2005; 102: 2180–5.

Aviner R, Geiger T, Elroy-Stein O. Genome-wide identification and quantification of protein synthesis in cultured cells and whole tissues by puromycin-associated nascent chain proteomics (PUNCH-P). Nat Protoc 2014; 9: 751–60.

Avni D, Biberman Y, Meyuhas O. The 5′ terminal oligopyrimidine tract confers translational control on top mRNAs in a cell type- and sequence context-dependent manner. Nucleic Acids Res 1996; 25: 995–1001.

Baleriola J, Walker CA, Jean YY, Crary JF, Troy CM, Nagy PL et al. Axonally synthesized ATF4 transmits a neurodegenerative signal across brain regions. Cell 2014; 158: 1159–72.

Beretta L, Gingras AC, Svitkin YV, Hall MN, Sonenberg N. Rapamycin blocks the phosphorylation of 4E-BP1 and inhibits cap-dependent initiation of translation. EMBO J 1996; 15: 658–64.

Berger SM, Fernandez-Lamo I, Schonig K, Fernandez Moya SM, Ehses J, Schieweck R et al. Forebrain-specific, conditional silencing of Staufen2 alters synaptic plasticity, learning, and memory in rats. Genome Biol 2017; 18: 222.

Bibb JA, Yan Z, Svenningsson P, Snyder GL, Pieribone VA, Horiuchi A, et al. Severe deficiencies in dopamine signaling in presymptomatic Huntington's disease mice. Proc Natl Acad Sci USA 2000; 97: 6809–14.

Bowles KR, Jones L. Kinase signalling in Huntington's Disease. J Huntingtons Dis 2014; 3: 89–123.

Braz BY, Belforte JE, Murer MG, Galinanes GL. Properties of the corticostriatal long term depression induced by medial prefrontal cortex high frequency stimulation in vivo. Neuropharmacology 2017; 121: 278–86.

Brunn GJ, Fadden P, Haystead TA, Lawrence JCJ. The mammalian target of rapamycin phosphorylates sites having a (Ser/Thr)-Pro motif and is activated by antibodies to a region near its COOH terminus. J Biol Chem 1997; 272: 32547–50.

Buren C, Parsons MP, Smith-Dijak A, Raymond LA. Impaired development of cortico-striatal synaptic connectivity in a cell culture model of Huntington's disease. Neurobiol Dis 2016; 87: 80–90.

Cepeda C, Hurst RS, Calvert CR, Hernández-Echeagaray E, Nguyen OK, Jocoy E, et al. Transient and progressive electrophysiological

[12.7.2019–7:09pm] [1–19] Paper: OP-BRAI190237
SUBJECT CATEGORY: ORIGINAL ARTICLE MANUSCRIPT CATEGORY: ORIGINAL ARTICLE

alterations in the corticostriatal pathway in a mouse model of Huntington's disease. J Neurosci 2003; 23: 961–9.

Chan AYM, Soltys C-LM, Young ME, Proud CG, Dyck, JRB. Activation of AMP-activated protein kinase inhibits protein synthesis associated with hypertrophy in the cardiac myocyte. J Biol Chem 2004; 279: 32771–9.

Chou JS, Chen CY, Chen YL, Weng YH, Yeh TH, Lu CS, et al. (G2019S) LRRK2 causes early-phase dysfunction of SNpc dopaminergic neurons and impairment of corticostriatal long-term depression in the PD transgenic mouse. Neurobiol Dis 2014; 68: 190–9.

Creus-Muncunill J, Rué L, Alcalá-Vida R, Badillos-Rodríguez R, Romaní-Aumedes J, Marco S, et al. Increased levels of rictor prevent mutant huntingtin-induced neuronal degeneration. Mol Neurobiol 2018; 55: 7728–42.

Cummings DM, Milnerwood AJ, Dallérac GM, Waights V, Brown JY, Vatsavayai SC, et al. Aberrant cortical synaptic plasticity and dopaminergic dysfunction in a mouse model of Huntington's disease. Hum Mol Genet 2006; 15: 2856–68.

Dang MT, Yokoi F, Cheetham CC, Lu J, Vo V, Lovinger DM, et al. An anticholinergic reverses motor control and corticostriatal LTD deficits in Dyt1 DeltaGAG knock-in mice. Behav Brain Res 2012; 226: 465–72.

Desplats PA, Kass KE, Gilmartin T, Stanwood GD, Woodward EL, Head SR, et al. Selective deficits in the expression of striatal-enriched mRNAs in Huntington's disease. J Neurochem 2006; 96: 743–57.

Di Pardo A, Amico E, Favellato M, Castrataro R, Fucile S, Squitieri F, et al. FTY720 (fingolimod) is a neuroprotective and disease-modifying agent in cellular and mouse models of huntington disease. Hum Mol Genet 2014; 23: 2251–65.

Fernández-Nogales M, Hernández F, Miguez A, Alberch J, Ginés S, Pérez-Navarro E, et al. Decreased glycogen synthase kinase-3 levels and activity contribute to Huntington's disease. Hum Mol Genet 2015; 24: 5040–52.

Gardner TW, Abcouwer SF, Losiewicz MK, Fort PE. Phosphatase control of 4E-BP1 phosphorylation state is central for glycolytic regulation of retinal protein synthesis. Am J Physiol Endocrinol Metab 2015; 309: E546–56.

Gingras AC, Gygi SP, Raught B, Polakiewicz RD, Abraham RT, Hoekstra MF, et al. Regulation of 4E-BP1 phosphorylation: a novel two step mechanism. Genes Dev 1999; 13: 1422–37.

Giralt A, Saavedra A, Carretón O, Xifró X, Alberch J, Pérez-Navarro E. Increased PKA signaling disrupts recognition memory and spatial memory: Role in Huntington's disease. Hum Mol Genet 2011; 20: 4232–47.

Gkogkas CG, Khoutorsky A, Ran I, Rampakakis E, Nevarko T, Weatherill DB, et al. Autism-related deficits via dysregulated eIF4E-dependent translational control. Nature 2013; 493: 371–7.

Goo CK, Lim HY, Ho QS, Too HP, Clement MV, Wong KP. PTEN/Akt signaling controls mitochondrial respiratory capacity through 4E-BP1. PLoS One 2012; 7: e45806.

Gruart A, Muñoz MD, Delgado-Garcia, JM. Involvement of the CA3-CA1 synapse in the acquisition of associative learning in behaving mice. J Neurosci 2006; 26: 1077–87.

Han I, You Y, Kordower JH, Brady ST, Morfini GA. Differential vulnerability of neurons in Huntington's disease: the role of cell type-specific features. J Neurochem 2010; 113: 1073–91.

Heesom KJ, Gampel A, Mellor H, Denton RM. Cell cycle-dependent phosphorylation of the translational repressor eIF-4E binding protein-1 (4E-BP1). Curr Biol 2001; 11: 1374–9.

Herbst EA, Holloway GP. Exercise training normalizes mitochondrial respiratory capacity within the striatum of the R6/1 model of Huntington's disease. Neuroscience 2015; 303: 515–23.

Hervás D, Fornés-Ferrer V, Gómez-Escribano AP, Sequedo MD, Peiró C, Millán JM, et al. Metformin intake associates with better cognitive function in patients with Huntington's disease. PLoS One 2017; 12: 1–11.

Hintiryan H, Foster NN, Bowman I, Bay M, Song MY, Gou L, et al. The mouse cortico-striatal projectome. Nat Neurosci 2016; 19: 1100–14.

Imai Y, Gehrke S, Wang HQ, Takahashi R, Hasegawa K, Oota E, et al. Phosphorylation of 4E-BP by LRRK2 affects the maintenance of dopaminergic neurons in Drosophila. EMBO J 2008; 27: 2432–43.

Ito H, Ichiyanagi O, Naito S, Bilim VN, Tomita Y, Kato T, et al. GSK-3 directly regulates phospho-4EBP1 in renal cell carcinoma cell-line: an intrinsic subcellular mechanism for resistance to mTORC1 inhibition. BMC Cancer 2016; 16: 1–12.

Jefferies HB, Reinhard C, Kozma SC, Thomas G. Rapamycin selectively represses translation of the "polypyrimidine tract" mRNA family. Proc Natl Acad Sci USA 1994; 91: 4441–5.

Jin J, Gu H, Anders NM, Ren T, Jiang M, Tao M, et al. Metformin protects cells from mutant huntingtin toxicity through activation of AMPK and modulation of mitochondrial dynamics. Neuromol Med 2016; 18: 581–92.

Jodeiri Farshbaf M, Ghaedi K. Huntington's disease and mitochondria. Neurotox Res 2017; 32: 518–29.

Jones TR, Kang IH, Wheeler DB, Lindquist RA, Papallo A, Sabatini DM, et al. CellProfiler analyst: data exploration and analysis software for complex image-based screens. BMC Bioinform 2008; 9: 482.

Jurado-Parras MT, Gruart A, Delgado-Garcia JM. Observational learning in mice can be prevented by medial prefrontal cortex stimulation and enhanced by nucleus accumbens stimulation. Learn Mem 2012; 19: 99–106.

King MA, Hands S, Hafiz F, Mizushima N, Tolkovsky AM, Wyttenbach A. Rapamycin inhibits polyglutamine aggregation independently of autophagy by reducing protein synthesis. Mol Pharmacol 2008; 73: 1052–63.

Kreiner G. Compensatory mechanisms in genetic models of neurodegeneration: are the mice better than humans? Front Cell Neurosci 2015; 9: 1–6.

Kumar A, Ratan RR. Oxidative stress and Huntington's disease: the good, the bad, and the ugly. J Huntingtons Dis 2016; 5: 217–37.

Labbadia J, Morimoto RI. Huntington's disease: underlying molecular mechanisms and emerging concepts. Trends Biochem Sci 2013; 38: 378–85.

Lawrence JCJ, Fadden P, Haystead TA, Lin TA. PHAS proteins as mediators of the actions of insulin, growth factors and cAMP on protein synthesis and cell proliferation. Adv Enzyme Regul 1997; 37: 239–67.

Lee E, Ryu HG, Kim S, Lee D, Jeong YH, Kim KT. Glycogen synthase kinase 3β suppresses polyglutamine aggregation by inhibiting vaccinia-related kinase 2 activity. Sci Rep 2016; 6: 1–10.

Lee, JH, Tecedor L, Chen YH, Monteys AM, Sowada MJ, Thompson LM, et al. Reinstating aberrant mTORC1 activity in huntington's disease mice improves disease phenotypes. Neuron 2015; 85: 303–15.

Li X, Alafuzoff I, Soininen H, Winblad B, Pei JJ. Levels of mTOR and its downstream targets 4E-BP1, eEF2, and eEF2 kinase in relationships with tau in Alzheimer's disease brain. FEBS J 2005; 272: 4211–20.

Lim NKH, Hung LW, Pang TY, Mclean CA, Liddell JR, Hilton JB, et al. Localized changes to glycogen synthase kinase-3 and collapsin response mediator protein-2 in the Huntington's disease affected brain. Hum Mol Genet 2014; 23: 4051–63.

Luthi-Carter R, Strand A, Peters NL, Solano SM, Hollingsworth ZR, Menon AS, et al. Decreased expression of striatal signaling genes in a mouse model of Huntington's disease. Hum Mol Genet 2000; 9: 1259–71.

Madronal N, Gruart A, Delgado-Garcia JM. Differing presynaptic contributions to LTP and associative learning in behaving mice. Front Behav Neurosci 2009; 3: 7.

Martin JB, Gusella JF. Huntington's disease. Pathogenesis and management. N Engl J Med 1986; 315: 1267–76.

[12.7.2019–7:09pm] [1–19] Paper: OP-BRAI190237
SUBJECT CATEGORY: ORIGINAL ARTICLE MANUSCRIPT CATEGORY: ORIGINAL ARTICLE

Martin I, Abalde-Atristain L, Kim JW, Dawson TM, Dawson VL. Abberant protein synthesis in G2019S LRRK2 drosophila parkinson disease-related phenotypes. Fly (Austin) 2014b; 8: 165–9.

Martin I, Kim JW, Lee BD, Kang HC, Xu JC, Jia H, et al. Ribosomal protein s15 phosphorylation mediates LRRK2 neurodegeneration in parkinson's disease. Cell 2014a; 157: 472–85.

Meyuhas, O. Synthesis of the translational apparatus is regulated at the translational level. Eur J Biochem 2000; 267: 6321–30.

Miguez A, García-Díaz Barriga G, Brito V, Straccia M, Giralt A, Ginés S, et al. Fingolimod (FTY720) enhances hippocampal synaptic plasticity and memory in Huntington's disease by preventing p75NTR up-regulation and astrocyte-mediated inflammation. Hum Mol Genet 2015; 24: 4958–70.

Milnerwood AJ, Cummings DM, Dallérac GM, Brown JY, Vatsavayai SC, Hirst MC, et al. Early development of aberrant synaptic plasticity in a mouse model of Huntington's disease. Hum Mol Genet 2006; 15: 1690–703.

Moerke NJ, Aktas H, Chen H, Cantel S, Reibarkh MY, Fahmy A, et al. Small-molecule inhibition of the interaction between the translation initiation factors eIF4E and eIF4G. Cell 2007; 128: 257–67.

Morita M, Gravel SP, Chénard V, Sikström K, Zheng L, Alain T, et al. MTORC1 controls mitochondrial activity and biogenesis through 4E-BP-dependent translational regulation. Cell Metab 2013; 18: 698–711.

Musa J, Orth MF, Dallmayer M, Baldauf M, Pardo C, Rotblat B, et al. Eukaryotic initiation factor 4E-binding protein 1 (4E-BP1): a master regulator of mRNA translation involved in tumorigenesis. Oncogene 2016; 35: 4675–88.

Nanahoshi M, Nishiuma T, Tsujishita Y, Hara K, Inui S, Sakaguchi N, et al. Regulation of protein phosphatase 2A catalytic activity by alpha4 protein and its yeast homolog Tap42. Biochem Biophys Res Commun 1998; 251:520–6.

Nho RS, Peterson M. Eukaryotic translation initiation factor 4E binding protein 1 (4EBP-1) function is suppressed by Src and protein phosphatase 2A (PP2A) on extracellular matrix. J Biol Chem 2011; 286: 31953–65.

Okunishi K, DeGraaf AJ, Zaslona Z, Peters-Golden M. Inhibition of protein translation as a novel mechanism for prostaglandin E2 regulation of cell functions. FASEB J 2014; 28: 56–66.

Osterweil EK, Krueger DD, Reinhold K, Bear MF. Hypersensitivity to mGluR5 and ERK1/2 leads to excessive protein synthesis in the hippocampus of a mouse model of fragile X syndrome. J Neurosci 2010; 30: 15616–27.

Parievsky A, Moore C, Kamdjou T, Cepeda C, Meshul CK, Levine MS. Differential electrophysiological and morphological alterations of thalamostriatal and corticostriatal projections in the R6/2 mouse model of Huntington's disease. Neurobiol Dis 2017; 108: 29–44.

Parker WD Jr, Boyson SJ, Luder AS, Parks JK. Evidence for a defect in NADH: ubiquinone oxidoreductase (complex I) in Huntington's disease. Neurology 1990, 40: 1231–4.

Pause A, Belsham GJ, Gingras AC, Donze O, Lin TA, Lawrence JCJ, et al. Insulin-dependent stimulation of protein synthesis by phosphorylation of a regulator of 5'-cap function. Nature 1994; 371: 762–7.

Pelegrí C, Duran-Vilaregut J, del Valle J, Crespo-Biel N, Ferrer, I, Pallàs M, et al. Cell cycle activation in striatal neurons from Huntington's disease patients and rats treated with 3-nitropropionic acid. Int J Dev Neurosci 2008; 26: 665–71.

Pryor WM, Biagioli M, Shahani N, Swarnkar S, Huang WC, Page DT, et al. Huntingtin promotes mTORC1 signaling in the pathogenesis of Huntington's disease. Sci Signal 2014; 7: 1–13.

Puigdellívol M, Cherubini M, Brito V, Giralt A, Suelves N, Ballesteros J, et al. A role for Kalirin-7 in corticostriatal synaptic dysfunction in Huntington's disease. Hum Mol Genet 2015; 24: 7265–85.

Rangel-Barajas C, Rebec G V. Dysregulation of corticostriatal connectivity in Huntington's disease: a role for dopamine modulation. J Huntingtons Dis 2016; 5: 303–31.

Ravikumar B, Vacher C, Berger Z, Davies JE, Luo S, Oroz LG, et al. Inhibition of mTOR induces autophagy and reduces toxicity of polyglutamine expansions in fly and mouse models of Huntington disease. Nat Genet 2004; 36: 585–95.

Reiter AK, Bolster DR, Crozier SJ, Kimball SR, Jefferson LS. AMPK represses TOP mRNA translation but not global protein synthesis in liver. Biochem Biophys Res Commun 2008; 374: 345–50.

Rosenwald IB, Kaspar R, Rousseau D, Gehrke L, Leboulch P, Chen JJ, et al. Eukaryotic translation initiation factor 4E regulates expression of cyclin D1 at transcriptional and post-transcriptional levels. J Biol Chem 1995; 270: 21176–80.

Rué L, López-Soop G, and Gelpi, E, Martínez-Vicente M, Alberch J, Pérez-Navarro E. Brain region-and age-dependent dysregulation of p62 and NBR1 in a mouse model of Huntington's disease. Neurobiol Dis 2013; 52: 219–28.

Saavedra A, García-Martínez JM, Xifró X, Giralt A, Torres-Peraza JF, Canals JM, et al. PH domain leucine-rich repeat protein phosphatase 1 contributes to maintain the activation of the PI3K/Akt prosurvival pathway in Huntington's disease striatum. Cell Death Differ 2010; 17: 324–35.

Saavedra A, Giralt A, Rué L, Xifró X, Xu J, Ortega Z, et al. Striatal-enriched protein tyrosine phosphatase expression and activity in Huntington's disease: a STEP in the resistance to excitotoxicity. J Neurosci 2011; 31: 8150–62.

Santini E, Huynh TN, MacAskill AF, Carter AG, Pierre P, Ruggero D, et al. Exaggerated translation causes synaptic and behavioural aberrations associated with autism. Nature 2013; 493: 411–5.

Santini E, Huynh TN, Longo F, Koo SY, Mojica E, D'Andrea L, et al. Reducing eIF4E-eIF4G interactions restores the balance between protein synthesis and actin dynamics in fragile X syndrome model mice. Sci Signal 2017; 10: 41–6.

Schiefer J, Sprünken A, Puls C, Lüesse HG, Milkereit A, Milkereit E, et al. The metabotropic glutamate receptor 5 antagonist MPEP and the mGluR2 agonist LY379268 modify disease progression in a transgenic mouse model of Huntington's disease. Brain Res 2004; 1019: 246–54.

Schmidt EK, Clavarino G, Ceppi M, Pierre P. SUnSET, a nonradioactive method to monitor protein synthesis. Nat Methods 2009; 6: 275–7. AQ7

Sharma A, Hoeffer CA, Takayasu Y, Miyawaki T, McBride SM, Klann E, et al. Dysregulation of mTOR signaling in fragile X syndrome. J Neurosci 2010; 30: 694–702.

Simmons DA. Modulating neurotrophin receptor signaling as a therapeutic strategy for Huntington's disease. J Huntingtons Dis 2017; 6: 303–25.

Slomnicki LP, Pietrzak M, Vashishta A, Jones J, Lynch N, Elliot S, et al. Requirement of neuronal ribosome synthesis for growth and maintenance of the dendritic tree. J Biol Chem 2016; 291: 5721–39.

Tain LS, Mortiboys H, Tao RN, Ziviani E, Bandmann O, Whitworth AJ. Rapamycin activation of 4E-BP prevents parkinsonian dopaminergic neuron loss. Nat Neurosci 2009; 12: 1129–35.

The Huntington's Disease Collaborative Research Group. A novel gene containing a trinucleotide repeat that is expanded and unstable on Huntington's disease chromosomes. Cell 1993; 72: 971–83.

Topol A, English JA, Flaherty E, Rajarajan P, Hartley BJ, Gupta S, et al. Increased abundance of translation machinery in stem cell-derived neural progenitor cells from four schizophrenia patients. Transl Psychiatry 2015; 5: e662.

Tyebji S, Saavedra A, Canas PM, Pliassova A, Delgado-García JM, Alberch J, et al. Hyperactivation of D1 and A2A receptors contributes to cognitive dysfunction in Huntington's disease. Neurobiol Dis 2015; 74: 41–57.

Valencia A, Reeves PB, Sapp E, Li X, Alexander J, Kegel KB, et al. Mutant huntingtin and glycogen synthase kinase 3-β accumulate in neuronal lipid rafts of a presymptomatic knock-in mouse model of Huntington's disease. J Neurosci Res 2010; 88: 179–90.

[12.7.2019–7:09pm] [1–19] Paper: OP-BRAI190237
SUBJECT CATEGORY: ORIGINAL ARTICLE MANUSCRIPT CATEGORY: ORIGINAL ARTICLE

van Dellen A, Welch J, Dixon RM, Cordery P, York D, Styles P, et al. N-Acetylaspartate and DARPP-32 levels decrease in the corpus striatum of Huntington's disease mice. Neuroreport 2000; 11: 3751–7.

Vázquez-Manrique RP, Farina F, Cambon K, Dolores Sequedo M, Parker AJ, Millán JM, et al. AMPK activation protects from neuronal dysfunction and vulnerability across nematode, cellular and mouse models of huntington's disease. Hum Mol Genet 2015; 25: 1043–58.

Villalonga P, Fernández de Mattos S, Ridley AJ RhoE inhibits 4E-BP1 phosphorylation and eIF4E function impairing cap-dependent translation. J Biol Chem 2009; 284: 35287–96.

Wang X, Proud CG. The mTOR pathway in the control of protein synthesis. Physiology 2006; 21: 362–9.

Wiseman SL, Shimizu Y, Palfrey C, Nairn AC. Proteasomal degradation of eukaryotic elongation factor-2 kinase (EF2K) is regulated by cAMP-PKA signaling and the SCFβTRCP ubiquitin E3 ligase. J Biol Chem 2013; 288: 17803–11.

Yang Y, Huang Q, Lu Y, Li X, Huang S. Reactivating PP2A by FTY720 as a novel therapy for AML with C-KIT tyrosine kinase domain mutation. J Cell Biochem 2012; 113: 1314–22.

Zid BM, Rogers AN, Katewa SD, Vargas MA, Kolipinski MC, Lu TA, et al. 4E-BP extends lifespan upon dietary restriction by enhancing mitochondrial activity in Drosophila. Cell 2009; 139: 149–60.